Short Term, Low Strain Radial Tensile Stiffness of a Triaxial Geogrid with Integral Junctions

by

Paul Stowell

A thesis submitted in fulfilment of the degree of Master of Philosophy

Volume I

University of Nottingham
Nottingham, UK

2020

ABSTRACT

This work starts by introducing the triaxial geogrid to be tested, TriAx®, along with its intended use and applications. It identifies that stabilisation and interlock is well understood but the radial, low-strain, tensile load-strain stiffness of these geogrids is not. A detailed review of the development of geogrids with integral junctions is then undertaken, highlighting how geogrids were first produced in the 1950's and how they have been developed up to the point of starting this work. Index and performance testing of geogrids with integral junctions are described. The specific geogrid for testing, TriAx® TX160, is introduced along with the methods of testing and the test programmes defined. Q.C., Index, and uniaxial creep testing is defined, carried out, and the data analysed and compared. A secondary crystallisation mechanism is established and occurs over time after production. Quadrant radial creep testing of TriAx® TX160 geogrid is introduced. To date wide-width, uniaxial constant rate of strain (CRS) tensile tests carried out in multiple directions have been used to determine the radial stiffness property, but the validity of this approach has not been investigated. Therefore, a new, in-plane, radial tensile test apparatus and test methodology has been developed for this purpose. The apparatus and sample geometry are defined, and the test data and analysis presented. All low strain behaviour from the three different test methodologies, constant rate of strain, uniaxial creep, and radial creep, were combined and compared with a possible "locked-in stress" being identified. The data from all three test methodologies are replotted with the possible locked-in stress. Upon comparing data obtained from this new radial tensile test and multi-directional uniaxial tensile testing, the data was found to be closely correlated. Thus, the multi-directional, uniaxial CRS tensile test is shown to be a reasonable and conservative means of determining the short-term, low-strain, radial tensile stiffness of multi-axial geogrids and the need for more elaborate testing methodologies is not required.

ACKNOWLEDGEMENTS

I am profoundly grateful to Prof Alan McGown and Chris Jenner for their continued support and advice. Alan and Chris have not only been my mentors but also my friends. I have learned many invaluable lessons from them over the years on how to conduct research and how to write a thesis and this will never be forgotten.

My further appreciation goes to Prof Nick Thom for acting as my supervisor and keeping me and my progress on track.

Thank you to my employers, Tensar International, and my manager, Mr. Anthony Walsh, for giving me the opportunity and the support to carry out this research. I would also like to thank my work colleges for providing support and information where needed.

TABLE OF CONTENTS

	PAGE NO.
VOLUME I	
ABSTRACT	**i**
ACKNOWLEDGEMENTS	**ii**
TABLE OF CONTENTS	**iii**
TERMS AND DEFINITONS	**viii**
Chapter 1: Introduction	
1.1 Background	1
1.2 Identification of the Problems	4
1.3 Aims of the Study	5
1.4 Objectives of the Study	6
1.5 Layout of Thesis	6
Chapter 2: Development and Properties of Geogrids with Integral Junctions	
2.1 Introduction	8
2.2 The First Generation of Geogrid Products	10
2.2.1 Uniaxial Geogrids	10
2.2.2 Biaxial Geogrids	10

2.3 Further Geogrid Product Development 12
2.3.1 Uniaxial Geogrids 12
2.3.2 Biaxial Geogrids 14
2.3.3 Triaxial Geogrids 16

Chapter 3: Review of Tensile Testing of Geogrids with Integral Junctions

3.1 Introduction 20

3.2 Index Tensile Testing of Uniaxial Geogrids 22
3.2.1 Methodology and Analysis 22
3.2.2 Typical Index Properties of Uniaxial Geogrids 23

3.3 Performance Tensile Testing of Uniaxial Geogrids 23
3.3.1 Methodology and Analysis 23
3.3.2 Typical Performance Properties of Uniaxial Geogrids 24

3.4 Index Tensile Testing of Biaxial Geogrids 24
3.4.1 Methodology and Analysis 24
3.4.2 Typical Uniaxial and Biaxial Index Properties of Biaxial Geogrids 25

3.5 Performance Tensile Testing of Biaxial Geogrids 26
3.5.1 Methodology and Analysis 26
3.5.2 Typical Performance Properties of Biaxial Geogrids 27

3.6 Index Tensile Testing of Triaxial Geogrids 27
3.6.1 Methodology and Analysis 27
3.6.2 Index Properties of Triaxial Geogrids 28

3.7 Performance Tensile Testing of Triaxial Geogrids 29
3.7.1 Methodology and Analysis 29

3.8 Defects of Testing Methods 29

Chapter 4: Methods and Programme of Testing TriAx® Geogrid TX160

4.1 Introduction 31

4.2 Physical Properties 21

4.3 Uniaxial Wide-Width QC, Index and Creep Test Methods 32

4.4 Quadrant Radial Creep Test Methods 32

4.5 Test Programme 32
- 4.5.1 Q.C Testing 32
- 4.5.2 Index Testing 34
- 4.5.3 Uniaxial Creep Testing 35
- 4.5.4 Quadrant Radial Creep Testing 35

Chapter 5: Uniaxial Q.C, Index and Creep Testing of TriAx® Geogrid – TX160

5.1 Introduction 36

5.2 QC and Index Testing 36
- 5.2.1 QC Test Data 36
- 5.2.2 Index Test Data 37
- 5.2.3 Comparison of QC and Index Test Data 37
- 5.2.4 Comparison of QC and Index Test Data to Declared Values 39
- 5.2.5 The Relationships Between Secant Stiffness, Maximum Load and Strain at Maximum Load 40
- 5.2.6 Influence of Strain Rates 40

5.3 Uniaxial Creep Testing 41
- 5.3.1 Introduction 41
- 5.3.2 Uniaxial Creep Test Data 42
- 5.3.3 Analysis of Creep Test Data 42

5.4 Comparison of Creep and CRS Test Data 43

5.5 Discussion 44

Chapter 6: Radial Creep Testing of TriAx® Geogrid – TX160

6.1 Background 45

6.2 Quadrant Radial Creep Testing 45
6.2.1 Introduction 45
6.2.2 Variations of Loads and Strains within Radial Test Specimens 47
6.2.3 Quadrant Radial Creep Test Data 49
6.2.4 Analysis of Creep Test Data 49

6.3 Discussion 50

Chapter 7: Low Strain Behaviour of TriAx® Geogrid – TX160

7.1 Introduction 51

7.2 CRS, Uniaxial Creep and Radial Creep Behaviour 51

7.3 Locked-In Stress 52

7.4 Discussion 53

Chapter 8: Summary, Discussion & Conclusions

8.1 Summary 55

8.2 Discussion 57

8.3 Conclusions 59

Recommendations for Future Research 61

References 62

Appendices

Appendix A1 – Uniaxial Q.C and Index Testing 68

Appendix A2 – Uniaxial Creep Testing 77

Appendix A3 – Radial Creep Testing 85

Tables, Figures, and Plates Volume II

TERMS AND DEFINITIONS

Amorphous: The lack of an ordered structure in a polymeric material.

Apertures: The openings in a grid structure.

Biaxial Geogrids: Geogrids which have been biaxially-oriented, meaning the geogrid has been stretched in two directions and generally at right angles to each other.

Buckling: A mode of failure generally characterised by an unstable lateral material deflection due to compressive action on the element involved.

Carbon Black: A black pigment produced by the incomplete burning of natural gas or oil, which is used as a filler/additive in the plastics industry to provide ultra-violet protection and to facilitate nucleation during the process of polymers.

CRS: Constant rate of strain

CRS Test: The measurements of loads to develop a constant rate of deformation.

Creep Testing: The measurement of strain when subjected to a sustained load.

Crystallisation: The process associated with the partial alignment of the molecular chains.

Declared Values: The averages of the means of the specimens tested in each of the four directions. (Values relate to batches from two different product lines).

Extrusion: Compacting a plastic material into powder or granules in a uniform melt and forcing it through an orifice in a more or less continuous fashion to yield a desired shape. While held in this shape, the melt is cooled to a solid state.

Geosynthetic: A product, whose components are made from synthetic or natural polymer, in the form of a sheet, a strip or a three-dimensional

structure, used in contact with soil and/or other materials in geotechnical and civil engineering applications.

Geotextile: A planar product made from synthetic or natural polymer used in contact with soil and/or other materials in geotechnical and civil engineering applications. It may be made by woven, non-woven or knitting processes.

Geogrid: A planar product made from synthetic or natural polymer used in contact with soil and/or other materials in geotechnical and civil engineering applications. It consists of a regular open network of connected tensile elements which may be linked by heat bonding, friction welding, interlacing or integral junctions. Such products may be formed as uniaxial, biaxial or multi-axial structures.

Grooving: Depressions in a film or sheet of polymer causing a change in the cross-sectional area.

HDPE: High Density Polyethylene, which has a density of over 0.94 and possessing relatively long molecular chains with few side branches.

Index Testing: Test data obtained by carrying out CRS tensile testing on batches that have been left for a period of time.

Interlock: The restriction of the movement of particulate matter which penetrate into the openings of a grid-like structure which exhibits tensile stiffness.

In-plane Testing: Testing where the load is applied parallel to the surface of the specimen.

Junctions: The structural component of a biaxial or multi-axial grid that connects the various sets of ribs.

Load: Applied Force

Locked-in Stress: Stresses existing within a material after plastic deformation has occurred, also referred to as residual stress.

Low Strain: Strain equal to or less than 0.5%

MD: The direction of manufacture of a geosynthetic product termed the Machine Direction.

Molecular Orientation: Creating a more orderly arrangement of polymer chains with respect to each other, thereby greatly increasing the stiffness / strength of the material.

Multi-axial Geogrids: Geogrids that have three or more directions.

Necking: Tensile deformation where relatively large amounts of strain localise disproportionately in a small region of the material.

Orientation: The alignment of the macro-molecules of polymeric materials to produce a highly-ordered structure.

Out-of Plane Testing: Testing were the load is applied perpendicular to the surface of the specimen.

Performance Testing: A physical test of a material in which to measure the performance characteristics.

Polymer: A chemical compound or mixture of compounds formed by polymerisation and consisting essentially of repeating structural units

Polypropylene: A thermoplastic polymer produced from polymerising propylene.

Q.C Testing: Test data obtained by carrying out CRS wide-width testing according to ISO10319 (2015) on various batches usually taken straight from production.

Radial Secant Stiffness: The secant stiffness measured at low strain values in defined radial directions.

Radial Secant Stiffness Ratio: The quotient of the minimum to the maximum Radial Secant Stiffness values. It represents the uniformity (isotropy) of the Radial Secant Stiffness of a product in all directions. A value close to 1.0 represents perfect isotropy - uniform in all directions.

Radial Strain: The strain measured from the LVDT of the quadrant radial creep test.

Reinforcement: The use of the stress-strain behaviour of a geosynthetic material to improve the mechanical properties of soil or other construction materials.

Rib: A rib is a tensile element that's connected to nodes or junctions

Screen Printing: A printing technique whereby a mesh is used to transfer ink onto a material.

Sheet: The starting material in which a geogrid is made.

Stabilisation: The function of stabilisation is provided by the interlocking of the aggregate with the geogrid and subsequent confinement of the particles. An additional effect of stabilisation and the aggregate confinement is the increase in modulus of the granular layer and its associated enhanced resilience, trafficking performance and load bearing capacity.

Stretching: The process by which geogrids are manufactured.

TAP: Time after production.

Tensioned Membrane Effect: decreasing the load induced in the subgrade soil by transferring the load to lateral zones.

Tolerances: Four standard deviations between the mean of the upper specification limit and the lower specification limit.

Triaxial Geogrids: Geogrids that have been oriented in three directions.

Uniaxial Geogrids: Geogrids that have been uniaxially-oriented, meaning the geogrid has been stretched in one direction.

XMD: The direction perpendicular to the direction of manufacture of a geosynthetic product termed the Cross-machine Direction.

1. Introduction

1.1 Background

The geosynthetics used in stabilisation structures (i.e. unpaved roads and unpaved areas) consist of mainly geotextiles and geogrids. Geocells are also used, but to a lesser extent.

Geotextiles were first used in subgrade stabilisation thanks to work in the late 1960s. Prof. Alan McGown was one of the earliest academics involved with geotextile testing and field implementation, McGown and Ozelton (1973). During the 1970s, geotextiles became extensively used in subgrade stabilisation applications (unpaved roads and unpaved areas).

Geotextiles can be separated into two major categories, Giroud (2009). (i) woven geotextile, i.e. individual threads, be it monofilaments, fibrillated yarns, slit films or other material, woven together. Although many different weaving methods and patterns exist, these products have yarns running longitudinally, and another in the transverse sense of the material; (ii) non-woven geotextiles, i.e. geotextiles manufactured by bonding materials (typically polypropylene and/or polyester) together, either through chemical or heat, needle punching or other methods, Koerner (2016). Examples of these geotextiles are shown in Figure 1.1 with some examples of geotextile manufacturers by category listed in Table 1.1.

Geogrids, first developed by Dr. Brian Mercer in the 1970s, appeared in subgrade stabilisation applications in the early 1980s. Since then, geogrids have been extensively used worldwide in subgrade stabilisation applications, and are often preferred in applications when limited deformations are required, especially when the geogrid-reinforced aggregate layer will be introduced into a paved road, Giroud (2009).

Giroud & Han (2004), explained that the differences between geotextiles and the geogrids is due to the difference in stress orientation which results from

the difference between geotextile-aggregate interface friction and geogrid-aggregate interlocking.

This interlocking mechanism between geogrid and aggregate plays a key role in the performance of a geogrid-reinforced stabilisation structure. Giroud (2009) and Lees (2020)

Geogrids can be separated into three major categories: (i) homogenous geogrids (commonly referred to as extruded, punched and drawn) typically manufactured from drawn polyethylene or polypropylene; (ii) woven geogrids, i.e. geogrids consisting of two sets of perpendicular woven ribs or yarns (often made of stretched polyester fibres) and then coated with PVC, latex or bitumen to provide dimensional stability and protection; (iii) welded geogrids, i.e. geogrids that consist of two sets of perpendicular straps, typically made of stretched polyester, welded at their junctions, Koerner (2009). Examples of these geogrid types are shown in Figure 1.2 with some examples of geogrid manufacturers by category listed in Table 1.2.

Since the arrival of geogrids in the early 1980's, biaxial geogrids have been the primary geogrid used for stabilisation structures until developments in the early 2000's saw the introduction of a new triaxial geogrid.

This thesis presents an assessment of the low-strain tensile behaviour of a new type of geogrid with integral junctions and possessing stretched ribs in three directions. It has been termed a "Triaxial Geogrid" with the registered trade mark TriAx®. This geogrid is intended for use in roads, railways and hard standings consisting of single or multiple layers of unbound aggregate. When the layers of these materials are subject to surface static or transient loading, vertical and horizontal components of stress develop within them. The horizontal components of stress cause the particles to move laterally and the function of the geogrid is to interlock with the particles and to restrict/minimise lateral movements. The application of geogrids in roads, railways and hard standings has been termed "Stabilisation" by EOTA (2012), and they have defined this as, "The beneficial consequence on the serviceability of an unbound granular layer, via the inhibition of the movement of the particles of the layer under load". They state that this is the

result of the mechanical effect of “Confinement” on an aggregate layer, resulting from the mechanism of “Interlock” provided by a stiff geogrid structure.

Giroud (2009) and Giroud and Han (2016) suggested that reconsideration of the strain mechanisms involved in pavement structures is required. In particular, they suggest that consideration should be given to the development of radial deformations at the sub-base/sub-grade interface, Fig 1.3, rather than the biaxial deformations as has been the case previously. Further, they suggested that the ability of these triaxial geogrids to restrict outward radial deformations at low strains rather at large strains in the pavement structures, will be their primary benefit.

Very much in line with the suggestions of Giroud (2009), European Technical Approval, EOTA (2012), has been given for the use of triaxial geogrids with integral junctions in applications involving the stabilisation of unbound granular layers. This approval has been given on the basis that their function is defined as the restriction of sub-base radial deformations. Further, they state that the critical properties of the triaxial geogrids are their radial tensile stiffness at low strains combined with their very high soil interaction coefficients.

The interlock mechanism of geogrids with integral junctions is well understood, Jewell et al (1984), Giroud et al (1984), Milligan and Love (1984), Konietzky et al (2004), Tutumluer and Al Qadi (2009). However, the radial, low-strain, tensile load-strain behaviour, (stiffness), of geogrids with integral junctions is less well established and little work has been undertaken for the new triaxial geogrids, hence the need to undertake this research study.

1.2 Identification of the Problems

Existing standards EN 13249:2016 and EN 13250:2016 recognise various functions for geotextiles and geotextile-related products; including the “Reinforcement” function, which depends upon the long term, relatively large strain, tensile load-strain behavior (stiffness) of geogrids. However, these standards do not identify the “Stabilisation” function and so do not refer to the low-strain, tensile load-strain behaviour, (stiffness) of geogrids. Further, these standards only take into account mechanical properties in the machine (MD) and cross-machine (XMD) directions of the geogrid and do not take account of the mechanical properties of triaxial geogrids in radial directions.

The intended use of triaxial geogrids is in stabilisation applications where the loading is radial, occurring at low strains and of short duration. Thus, in this application, it is the short term, radial tensile stiffness of the geogrid developed at low strains that is of importance. Rupture strength and its associated strain as mentioned in existing standards, such as the EN Standards 13249:2016 and EN 13250:2016, are useful parameters in production quality management and site verification but they are poor indicators of the performance of a triaxial geogrid when employed in the stabilisation application.

BS EN ISO 10318-1:2015+A1:2018 defines stabilisation as *“improvement of the mechanical behaviour of an unbound granular material by including one or more geosynthetic layers such that deformation under applied loads is reduced by minimizing movements of the unbound granular material”*

The definition helps reinforce that you do not want movement of the unbound granular materials, which is hard to achieve through pure friction.

In 2012 an EOTA Technical Report was developed, EOTA TR041 “Non-reinforcing hexagonal geogrid for the stabilisation of unbound granular layers by the way of interlock with the aggregate”. This EOTA report was developed by the approval body KIWA, who defined uniaxial tensile testing procedures for the determination of radial tensile stiffness through wide width (CRS) tensile testing. Since then, a great deal of work has gone into determining

these uniaxial Index (CRS) properties of triaxial geogrids, however, little or no work has been undertaken to determine their short term, radial, low strain, tensile load-strain (stiffness).

In the response to the need to identify the properties of triaxial geogrids in stabilisation applications, the work carried out in this thesis will include uniaxial QC, Index (CRS) and short term uniaxial and radial Creep testing. This testing will be carried out on a single roll of the most widely used triaxial geogrid, TriAx® TX160 in order to avoid the complications of product variability. The test data obtained from the uniaxial CRS and radial Creep test data will be correlated. The objective of this will be to link the radial, short term, low strain stiffness to the uniaxial, short term, low strain stiffness, in order to determine if a simple uniaxial testing method can be employed in the future to characterise the radial, load-strain behavior of triaxial geogrids used in stabilisation applications.

1.3 Aims of the Study

It is recognised that the critical properties of multi-axial geogrids, when used for the stabilisation of unbound granular materials, are their interlock capability and short-term, in-plane, low-strain, tensile stiffness in all radial directions. Their interlock characteristics are well understood, but not their short-term, low-strain radial tensile stiffness. To date wide-width, uniaxial constant rate of strain (CRS) tensile tests carried out in multiple directions have been used to determine this property, but the validity of this approach has not been investigated. The work set out in this thesis aims to develop a new, in-plane, radial tensile test apparatus and test methodology, with the test data obtained from this new radial tensile test to be compared to that obtained from multi-directional uniaxial tensile testing and to validate the wide-width CRS approach.

1.4 Objectives of the Study

Based on the aims of the study set out in the previous section, the objectives of the study are to:

1) Perform uniaxial QC, Index (CRS) and Performance (Creep) tests for TriAx® TX160 geogrids and analyse data.

2) Develop a new, in-plane, radial tensile test apparatus and test methodology suitable for TriAx® geogrids.

3) Perform radial Creep tests using the new, in-plane radial test apparatus on TriAx® TX160 geogrids and analyse the data.

4) Correlate the data obtained from uniaxial CRS and radial Creep tests.

5) Link the radial, short term, low strain stiffness to the uniaxial, short term, low strain stiffness, in order to validate the wide-width CRS approach as defined in the EOTA TR041.

1.5 Layout of Thesis

Chapter Two provides an insight into the history of geogrids, how they were manufactured and how they evolved. This chapter specifically deals with how the first extruded polymer mesh process, invented by Dr. Brian Mercer, went on to become an extrude, punch, and stretch process producing uniaxial and biaxial geogrids and how Mr. Anthony Walsh revolutionised the geogrid market by inventing the multi-axial geogrid, Triax®.

Chapter Three reviews the tensile testing of geogrids with integral junctions. It describes the methodology and analysis for index and performance testing of uniaxial, biaxial and triaxial geogrids.

Chapter Four describes the uniaxial wide-width Q.C, index and creep test methods, the radial 90° quadrant creep test methods, and programme of testing TriAx® geogrid TX160.

Chapter Five provides the uniaxial index and Q.C test data for TriAx® geogrid TX160 and the influence of strain rates, along with uniaxial creep test data, analysis and comparison of CRS and creep.

Chapter Six describes the radial creep testing of TriAx® geogrid TX160. It describes the radial specimen sizes, the variation of loads and strains within radial test specimens and provides the radial creep test data and analysis.

Chapter Seven compares the low strain behaviour of all three test methodologies, CRS, Uniaxial Creep, and Quadrant Radial Creep, used in this study. It identifies the presence of a locked-in stress and compares the data with and without the locked-in stress.

Chapter Eight contains a summary of the work undertaken, as well as the discussions and conclusions from the present study. Recommendations for future work are presented at the end of this chapter.

Appendices contain a detailed description of the testing protocols for Uniaxial Q.C and Index Testing, Uniaxial Creep Testing, and Quadrant Radial Creep Testing.

2. Development of Geogrids with Integral Junctions.

2.1 Introduction

During the mid-1970s the rapid increase in polymer raw material costs required that the manufacture of polymer products had to become more economical whilst maintaining or improving their quality. The innovative approach taken by Dr. F.B. Mercer of Netlon Ltd, was to develop manufacturing processes that involved molecular orientation of polymers, Mercer (1986).

The first extruded polymer mesh process developed by Mercer in the late 1950s consisted of extruding molten polymer through counter-rotating die lips, Fig 2.1. This produced a bi-planar mesh structure with junctions where two strands crossed in two distinct planes, Fig 2.2. Upon stretching these meshes, it proved difficult to produce orientation through the junction zone due to their bi-planar nature. This resulted in un-oriented polymer in the junctions and therefore “non-contributing” materials, Mercer (1986).

In the late 1970s, with molecular orientation and economy very much in mind, Mercer undertook research on a new product range. This research was based on producing oriented polymer products from uni-planar starting material by punching a precise pattern of holes in the starter sheet, heating the material and then stretching it, Fig 2.3.

This research showed that by uniaxial stretching in the machine or cross-machine direction, products with high tensile strength in one direction were produced. With stretching in both directions, products with high tensile strength in two orthogonal directions were produced. Thus, polymeric geogrids with integral junctions were developed, Mercer (1986).

The uni-directional products, with stretched ribs in one direction, were generally termed “Uniaxial” geogrids and the bi-directional products with stretched ribs in two directions were generally termed “Biaxial” geogrids.

The uniaxially stretched geogrids, proved to be most suitable in civil engineering applications such as soil retaining walls and embankments, where the induced forces and strains are essentially in one direction. The biaxially stretched geogrids proved to be most suitable in applications such as the sub-base of road pavements and in railway tracks, where the induced forces and strains are in at least two directions.

By the end of 1978, the initial research was completed and the concept of manufacturing polymer geogrids more economically through the process of molecular orientation was established.

Other developments took place through the years and saw the introduction of new products, still termed “Uniaxial” and “Biaxial” products. It wasn’t until 2002 that a totally new approach to the manufacture of geogrids came to light and new products which had stretched ribs in three directions were launched. These were termed “Triaxial Geogrids” and were to be given the trade mark TriAx®.

The molecular orientation mentioned above plays an important role in to the performance of geogrids. For uniaxial geogrids it provides high tensile strength and improved creep performance needed for reinforcing applications and for biaxial and triaxial geogrids it provides the tensile stiffness required to improve stabilisation applications. As mentioned in Chapter 1, the interlock mechanism plays a key role in the stabilisation performance of geogrids. Giroud (2009), identified factors that governed that geogrid-aggregate interlocking, these factors included the shape and stiffness of ribs, and stiffness (more than strength) of junction between ribs, hence the improved stiffness achieved from molecular orientation is important to how these geogrids perform.

2.2 The First Generation of Geogrid Products

2.2.1 Uniaxial Geogrids

The uniaxial geogrid products were granted patents internationally, e.g. in the UK Patent No. GB2073090, published 14/10/1981, P.L.G. Research Limited (1981).

This patent describes in detail the manufacturing process, which can be summarised as punching holes in a rectangular or square pattern into a cooled sheet of extruded polymer of at least 0.75mm thick and then uniaxially stretching it. The first uniaxial products so produced were designated as Tensar SR1 and Tensar SR2.

The Tensar SR2 product was manufactured from 4.5mm thick sheet, punched with 12.5mm diameter holes at 25mm centres and then stretched at a ratio of 4.5:1. Tensar SR1 had a much smaller aperture size but exhibited the same short-term tensile strength as SR2. The SR1 was intended to be used with smaller particle materials such as silts and clays but testing showed that the SR1 could not provide interlock with larger gravel sized fill. The range of products was therefore reduced to a single product, viz. Tensar SR2, Paul (1994). The geometry and physical properties of Tensar SR2 are given in Fig. 2.4.

2.2.2 Biaxial Geogrids

The biaxial geogrid products were also granted patents internationally, e.g. in the UK Patent No. GB2035191, published 18/06/1980, P.L.G. Research Limited (1980).

These biaxial geogrids were manufactured by punching holes in a rectangular or square pattern into a cooled sheet of extruded polymer of at least 0.75mm thick. The punched sheet was then stretched in two directions at right angles, so creating a biaxially stretched structure which has two orientated strands at right angles to each other, connected by orientated junctions and crotches.

Mercer (1986) noted that stretching in the second direction at right angles to the first direction caused “unusual and advantageous flow to take place”. The reason that this occurs is that the strands in the machine direction are held under tension and as the transverse direction strands are stretched the polymer is drawn around the four crotch zones of the junction. This creates high tear resistance and at the same time causes the crotch of the junction to be biaxially oriented. This molecular alignment is shown diagrammatically in Fig. 2.5.

These biaxial geogrids, as stated earlier, were designed to be used in applications such as the sub-base of road pavements and in railway tracks. Research carried out at the University of Oxford, in order to obtain the optimum interlock between biaxial geogrids and road sub-base materials, found that the optimal interlock was achieved when materials were used that contained particles which possessed a diameter in the range 0.2 to 1.5 times the aperture size of the geogrid, Milligan (1981).

Further manufacturing development trials were undertaken to determine the optimum punched hole pattern for these biaxial geogrids and during these, a problem was identified. The biaxial stretching process involves gripping the edges of uniaxially stretched sheet using clips attached to a pair of chains which diverge as they travel in the machine direction. As these chains diverge the grid gets stretched in the transverse direction forming the right angled transverse strands. The problem with this is that due to the large spherulites of polymer formed by the slow cooling of the thick sheet and because of the unequal cross section of the punched and uniaxially stretched sheet, stretching occurs in random locations across the width of the sheet. This proves difficult to control and makes it difficult to produce consistent aperture sizes, Paul (1994).

It was discovered that this problem could be rectified by pre-orienting the polymer in the strand forming zones by mechanically punching grooves into the punched sheet at a temperature well below its melting range, thus allowing products with a more regular geometry to be produced, Mercer (1986). This process was granted patents internationally, e.g. in the UK

Patent No. GB2128132, published 26/04/1984, P.L.G. Research Limited (1984).

Whilst all this research on grooving of the polymer sheet was taking place, different hole shapes and sizes were also investigated. The initial work was undertaken with round and square holes, with the square holes showing a significant benefit but with the axes turned through 45° producing a diamond shaped hole, Paul (1994). This is shown diagrammatically along with the grooving in Fig 2.6.

From the above and taking in to account the requirements for sub-base applications with regards to aperture size, two biaxial geogrids patterns were formed and in turn three products were produced, viz. Tensar SS1, SS2 and SS3.

Tensar SS1 was produced using 3mm square holes on a diamond pattern at 9mm centres in 3mm thick grooved polypropylene sheet. Tensar SS2 was produced using the same punch pattern formed in 4.5mm thick sheet and the larger aperture grid, Tensar SS3, was produced with 6mm square holes on a diamond pattern at 15mm centres in 4mm thick grooved polypropylene sheet. The geometries and physical properties of these products are given in Figs. 2.7 to 2.9.

2.3 Further Geogrid Product Development

By the early 1980's, the original manufacturing processes had been successfully employed to produce a range of geogrids suitable for all the civil engineering applications identified at that time and a full scale manufacturing plant with a high production capacity had been established. However, further development work was undertaken in order to expand and improve the products and extend the application range, Paul (1994)

2.3.1 Uniaxial Geogrids

A method known as "Screen Printing" was developed to provide further understanding of the effects of molecular orientation during stretching of the punched polymer sheet. Screen printing consists of printing the punched

sheet with a regular series of orthogonal lines, which can be seen in Plates 2.1 and 2.2. Once stretched the molecular orientation within the grid can be identified.

Plate 2.3 shows a stretched sample of the uniaxial Tensar SR2 product. This shows that the highest degree of molecular orientation occurs in the rib of the product with the orientation decreasing as it moves towards the junction. The centre of the rib is where the highest degree of molecular orientation is achieved. Some orientation occurs through the junction and this can be seen in detail in Plate 2.4.

During this development work, it was discovered that the orientation passing through the junction was limited to a very low level. Exceeding this limit caused a problem. The problem being that the junction zone was prone to cracking making the product less robust, Paul (1994).

Examination and measurement of the stretching pattern indicates that the centre of the rib has a draw ratio of around 9:1 with the adjacent areas having a reducing draw ratio until it reaches a minimum of a ratio of approximately 1:1 at the junction. At the point of maximum draw ratio (orientation) the cross-sectional area is at a minimum and stress at a maximum. This means that for any geogrid produced from a punched sheet with specific hole sizes and spacings, there is a maximum rib length that can be produced.

Punching holes in a sheet is essentially wasting material (although punch-out is recycled) and with Mercer's original concept in mind, of economy and molecular orientation, the way to minimise such waste is to draw the sheet as far as possible by producing the maximum area of finished product with the highest overall draw ratio (orientation) and in turn tensile strength. With all this in mind the development of a new hole shape, known as the "Diabolo", was undertaken, Fig 2.10.

The diabolo shaped hole produces Tensar SR-type geogrids but with longer ribs. The idea of the diabolo was to create two yield zones that would control the degree of orientation passing through the junction. This in turn allowed

for faster processing speeds without increasing the rate of strain in the yield zones as well as allowing for a greater overall draw ratio. Figure 2.11 shows a diagram of the diabolo punched sheet and the stretched sample with the two yield zones.

The original Tensar SR2 and the Diabolo shape punched product Tensar SR80, were intended to exhibit the same short term tensile strength of 80kN/m. By comparing the mass per square metre of the original Tensar SR2 at 850g/m2 with the Tensar SR80 at 700g/m2, the benefits the Diabolo punch produce became evident. The geometry of Tensar SR2 is shown in Fig. 2.4 and can be compared with Tensar SR80, shown in Fig. 2.12.

In parallel with the development of the Diabolo punch was the introduction of a new range of products using different sheet thicknesses. These products became known as Tensar SR55, SR80 and SR110. These geogrids share similar geometry and have short term tensile strengths of 55, 80 and 110kN/m.

Further, in the early 1990's a modification was made to the Diabolo punch. The punch length was increased to allow for a longer rib by spacing the two yield points further apart. Although a longer punch increased the amount of punch out, (which was recycled), the overall economy was increased further and a new wider range of products was developed. These products became the RE series and were designated as Tensar 40RE, 55RE, 80RE, 120RE and 160RE. The specifications of these products are given in Fig. 2.13.

In 2008, further development of the RE series was undertaken. This became the RE500 series and is made up of RE510, RE520, RE540, RE560, RE570 and RE580. The specifications of these products can be seen in Fig. 2.14.

2.3.2 Biaxial Geogrids

In the early 1980's biaxial geogrid developments were also under way. One application area identified for the use of biaxially stretched products was in asphalt layers in road pavements. A new product, Tensar AR1, was manufactured for this purpose.

Tensar AR1 was a heat-treated version of Tensar SS3. Both were manufactured from the same punched sheet, but heat treatment of the AR1 product was necessary as asphalt is laid at temperatures between 140°C and 180°C which is much higher than the temperature at which SS3 is manufactured and this would induce shrinkage, distortion and loss of orientation in the geogrid when placed in the asphalt. The heat treatment of the AR1 was carried out during the manufacturing process by employing a higher manufacturing temperature and using infra-red heaters at the end of the stretching process to heat set the product while holding it under tension to prevent reversion. This process allowed AR1 geogrids to be used with asphalt at temperatures up to 180ºC without much shrinkage taking place. The geometry and physical properties of AR1 are shown in Fig. 2.15.

Construction of roads, railways and working platforms over very soft foundations proved the need for even stronger biaxial geogrids than SS2. Paul (1994) describes how the Japanese market required a higher tensile strength product with small aperture sizes to be used in soft foundation applications such as estuarine mud with sand as the fill material. The Japanese believed that a smaller aperture sized grid would reduce the risk of mud squeezing up through the geogrids and in turn improve the interlock.

It was known that higher tensile strength geogrids could be achieved via additional stretching of the ribs but in doing so would create larger apertures and space the load carrying ribs further apart. Although this would achieve the higher tensile strength in the ribs the product strength per metre is reduced since the larger apertures reduce the number of ribs per meter. The solution was to use a co-polymer grade of polypropylene which gave the high strengths required at relatively low draw ratios. The product was designated Tensar SS35 and was produced form 6.1mm thick sheet punched with 3mm square holes on a diamond pattern at 10mm centres.

In the early 1990’s, development and upgrading of production machinery was carried out. One of the upgrades involved changes to the uniaxial stretching process and the use of a “Stenter”, (a diverging stretching mechanism), so that biaxial products could be made in one continuous process.

These developments allowed for a new range of biaxial geogrids to be manufactured. These biaxial geogrids had square apertures and essentially equal tensile strength in both the longitudinal and transverse directions. These grids were designated as Tensar SS20 and SS30, which went on to supersede Tensar SS1 and SS2, and also Tensar SS40 which superseded Tensar SS35. A typical specification of SS30 is shown in Fig 2.16.

Another development to take place was the introduction of geogrids with large apertures to supersede Tensar SS3. These products were Tensar SSLA20 and SSLA30.

Tensar SSLA20 and SSLA30 were both produced with the same punch shape and punch pattern but produced from different sheet thicknesses. 4.4mm and 7mm. These produced large aperture geogrids (65mm x 65mm) with equal short-term tensile strengths, of 20kN/m and 30kN/m, in machine and cross-machine directions. They were used in countries where large aggregate is employed, such as in Norway. They were also used in wind farm and ballast/track bed applications. Laminated composite versions of these grids, which consist of the geogrid laminated to a non-woven polypropylene geotextile, were also produced for asphalt applications and were designated as SSLA20-G and SSLA30-G. A typical specification of SSLA30 are shown in Figs. 2.17.

2.3.3 Triaxial Geogrids

In 2002 developments had begun on a completely new, step change in the manufacturing of geogrids with integral junctions.

The biaxial products have two directions in which the main strengthening of the product occurs, the machine and cross-machine directions, (0° and 90° respectively). This in-turn results in the physical properties of the structure to be optimal in these two directions. If the structure was to be tested at other angles between 0° and 90° or if torsion is applied, then it would be possible to identify weaknesses in the structure.

Walsh (2006) describes how developments led to incorporating a 45° angled rib within a square grid aperture creating a third direction of properties to be

defined. By so doing, geogrids with triangular apertures are produced instead of the normal square and rectangular ones. These triangular apertures in-turn produce a hexagonal repeat pattern within the geogrids. This hexagonal repeat pattern provides a structure with quasi-isotropic tensile strength properties in the plane of the geogrids, Walsh (2006).

These quasi-isotropic properties are apparent when comparisons are made between the properties of triaxial geogrids and biaxial geogrids by carrying out multi-directional tensile strength testing and plotting the test data in polar diagram form. These polar diagrams allow the response of the grid to be seen visually, not just in linear terms but as a 360° structure.

Figs. 2.18 to 2.20 show polar diagrams of short-term tensile strength data, (including ultimate strength, secant modulus and grid strength at 2% strain), for a biaxial and a triaxial product. It clearly shows that the biaxial geogrid is characterised by four distinct peaks corresponding to the machine and cross-machine, 0/180° and 90/270°, and much lower strengths in other directions, which illustrates the anisotropic nature of this type of structure. In contrast, the triaxial geogrid provides a quasi-isotropic response to imposed stresses and strain. Thus, the triaxial geogrid is more capable of carrying radial stresses and allows a more effective load distribution when subjected to wheeled vehicle loading or heavy point loading, Walsh (2006).

The manufacturing process is generally a biaxial process with the punch geometry consisting of a repeated cluster of six round holes punched into a polypropylene sheet, Fig. 2.21, that contains a master batch package, consisting of carbon black, anti-oxidants and the polypropylene homopolymer carrier.

Stretching of this type of punch configuration returns a geogrid with a geometry consisting of equilateral triangles that form a regular hexagon. This can be seen in Fig. 2.22.

To determine the correct aperture size of the geogrid, small scale trafficking trials were conducted at the University of Nottingham, UK. After many tests, it was determined that the most efficient aperture size for standard aggregate

sizes was 80AF, (where AF is the distance ‘across the flats’ of the hexagon, from centre to centre of the rib, with 80 being the distance in mm), Walsh (2006), Fig. 2.23.

The triaxial geogrid products were granted patents internationally, e.g. in the UK Patent No. GB2391832, published 18/02/2004, Tensar Technologies Limited (2004), and were termed “TriAx®” geogrids.

The launch of triaxial geogrids went ahead in 2007 with the first range of products being TX160, TX170 and TX180, which were solely produced in Wuhan, China. In December 2008 the Tensar UK plant began modifications to their biaxially stretched machinery to produce triaxial geogrids and was in production early 2009 producing the same TX160, TX170 and TX180 as in China. A typical technical data sheet for these products are shown in Fig. 2.24.

Development continued through 2009 with laminated composite versions of TX160 and TX170 products being introduced, in the UK only, for use in asphalt applications. Laminated composite version of TX180 were not made as a standard product. The identification of these products was distinguished with a ‘G’ after the product name, viz. TX160-G and TX170-G. A typical technical data sheet for these products are shown in Fig. 2.25.

Other developments in 2009 included a lighter weight product produced only for the UK market, and known as TX150. A laminated composite version, TX150-G, was also produced.

In 2011 a large aperture version was produced. This geogrid had an aperture of 120AF and was intended for applications in which large aggregate was used. A laminated composite, ‘G’ version, was also manufactured. A typical technical data sheet for these products are shown in Fig. 2.26.

In late 2009 development of a small aperture grid was carried out in the UK for construction over soft ground. This produced a geogrid with a smaller aperture size and was named TX130S. Once developed, the tooling was shipped to the Morrow Plant in the USA, where the product was launched early 2010. The same tool was then developed for the UK plant which saw

the launch of TX130S and TX130S-G into the UK market in 2012. Technical data for these products can be seen in Fig 2.27.

A new plant in Russia became operational in 2014 for the production and sales of triaxial geogrids for the Russian market.

3. Review of Tensile Testing of Geogrids with Integral Junctions.

3.1 Introduction

In-plane uniaxial constant rate of strain [CRS] tensile testing aims to determine the short term tensile strength properties of geosynthetic materials and is usually employed for manufacturing quality control purposes and specifications. Such tests are known as “Index Tests”, Murray & McGown (1982). In-plane uniaxial (CRS] testing for specification purposes is now well established for determining these Index properties and numerous National and International Standards exist, e.g. BS6906-Part 1 (1987), ASTM D6637-11 (2012) and ISO 10319 (2015). Long-term material properties relevant to the function of a geogrid in a particular application are known as “Performance” tests, Murray & McGown (1982). In-plane uniaxial sustained load (creep) tensile testing is now also well established for determining these properties and numerous National and International Standards exist, e.g. BS6906-Part 5 (1991) and ISO 13431 (1999).

In the early years of the development of testing methods for geosynthetics, out-of-plane uniaxial CRS, creep and repeated loading tests were suggested by various researchers as Index or as Performance test methods, e.g. Wilson-Fahmy (1981), Kabir (1984), McGown et al (1984), Yeo (1985), but these have never been fully developed to become National or International Standards

In-plane uniaxial test methods for determining the tensile Index and Performance properties of geogrids with integral junctions were first developed at the University of Strathclyde, McGown et al (1984). Specialised clamps were developed, as seen in Fig. 3.1, so that geogrids could be tested to determine their tensile load-strain properties. The uniaxial geogrids were held directly in the clamps by their top and bottom transverse bars whereas the biaxial geogrids had to be cast into the clamps using a low melting point alloy named “Ostalloy 158”, McGown et al (1984).

For biaxial geogrids, in-plane uniaxial testing was generally carried out in the machine and cross-machine directions. Attempts to combine the properties obtained in this manner proved to be problematic due to the data from the two directions involving vector quantities. Further, it was reported that conventional uniaxial tensile testing could not be used to reasonably predict material stiffness as the values were likely to be several times higher, Nimmersgern (1994). Therefore, Kupec (2004) suggested that biaxial geogrids needed to be reassessed under biaxial tensile loading conditions and developed both in-plane and out-of-plane, biaxial CRS and creep testing apparatuses and methods.

For triaxial geogrids, in-plane uniaxial short-term tensile testing was initially carried out in only the machine and cross-machine directions. However, Walsh (2006) quickly recognised that in order to properly assess this new type of geogrid, it was necessary to undertake testing in four directions, viz. in the two 'mid rib' directions (0° and 60° - with respect to the machine direction) and the two 'rib' directions (30° and 90° - with respect to the machine direction). Later, development work was undertaken at the University of Nottingham in relation to in-plane and out-of-plane Performance testing of triaxial geogrids, using CRS and repeated loading. This work identified new test protocols and apparatuses. As with biaxial geogrids, attempts to combine the properties of triaxial geogrids obtained in different directions, proved to be problematic due to the data involving vector quantities.

The outputs from all the methods identified above comes down to the difference between geogrid/stabilisation and geotextile/tensioned membrane. For geotextiles/tensioned membrane design of an unpaved road, tensile results in MD and XMD at strains of 2, 5, 10% and max strain can be used in an appropriate design

For TriAx®, the design should be based from factors derived from full scale testing, however, a suitable method to determine low strain radial behaviour (e.g. the methods proposed in this thesis) could be used to identify products which may be suitable for expensive full scale testing.

As mentioned in the previous chapters, it is tensile stiffness and geogrid-aggregate interlocking that are the important properties for extruded geogrids used in stabilisation applications. However, it is tensile strength that is most often mentioned in publications and specifications regarding geogrids.

“The use of tensile strength to characterise geogrids used in unpaved roads and unpaved areas is tempting because tensile strength is the simplest and most readily recognised (if not understood) mechanical property of a geosynthetic. Simplicity and recognition are not a justification for using a property. The property must be relevant”, Giroud (2009).

Giroud (2009), also explains that even when a geosynthetic is subjected to tensile forces in a stabilisation structure, the relevant property is not tensile strength but tensile stiffness, due to the fact the strains involved are generally not sufficient to mobilise the ultimate strength. Tests by Watts et al. (2004) interpreted by Giroud & Han (2006) show that geogrid strains under dual wheels are very small (i.e. between 0.1 and 1.2%) after full development of ruts at the end of the test.

The main reason tensile strength, as opposed to tensile stiffness, is irrelevant is not because of the small strains involved but that tensile strength is not applicable to geogrid-aggregate interaction.

3.2 Index Tensile Testing of Uniaxial Geogrids

3.2.1 Methodology and Analysis

For manufacturing quality control testing, in-plane uniaxial (CRS) testing has been used from the time of the development of the first uniaxial geogrids with integral junctions. However, the test methodology and test conditions were never widely published nor widely agreed.

For specification purposes in-plane uniaxial CRS tensile testing of uniaxial geogrids, McGown et al (1984), used a constant rate of strain of 2% per minute and standard material conditioning test conditions of 20°C ± 2°C and

65% ± 2% humidity to establish reference load strain properties for these geogrids.

Since this initial development work, Index testing standards for specification purposes have evolved, with the current testing standard for CE marking being ISO 10319 (2015). Typical test data are plotted as shown in Fig 3.2 and 3.3.

3.2.2 Typical Index Properties of Uniaxial Geogrids

Typical index properties for uniaxial geogrids are given in Table 3.1.

3.3 Performance Tensile Testing of Uniaxial Geogrids

3.3.1 Methodology and Analysis

The function of uniaxial geogrids in the range of applications in which they are employed is reinforcement and is directly related to the in-plane uniaxial time-dependant tensile strength/stiffness. McGown et al (1984) first explained how the long-term load-strain properties of uniaxial geogrids can be determined using in-plane rapid loading creep testing. The test methodology involves loading a geogrid quickly and smoothly (in less than 5 seconds), by way of a dead weight load or an adjustable 5 to 1 level arm system. The deformation of the test specimen is initially measured electronically and then changed over to mechanical dial gauges as the strain rate slows down. The data obtained are plotted as load against time and as strain against time using at least 5 levels of loading at various test temperatures. Test specimens are left under load in excess of 1000 hours, unless rupture occurred within that time period. Tests that do not rupture are terminated once the daily strain rate reaches an agreed minimum value or becomes insignificant. At the end of a test the specimen is partially unloaded and left under reduced sustained loading for 100 hours to establish the elastic recovery of the specimen. The unloading and reduced sustained loading are measured using the same techniques used during the loading stage.

Since this initial development work for determining long-term performance properties National and International Standards have evolved, with the current creep testing standard for CE marking being ISO 13431 (1999). Typical test data are plotted as shown in Figs. 3.4 and 3.5. The plots show creep performance for Tensar SR2 and Tensar RE560. The SR2 plot shows various linear creep curves for a range of loads tested at 20°C for 1000 hours, e.g. an applied load of 26.1 kN/m gave a strain of around 8.4% after 1000hours. The Tensar RE560 plot shows a strain versus log time creep curve when tested at 47.5% of its nominal ultimate strength at 40°C. The geogrid was tested to failure. The results show it reached a strain of around 39% after around 1700 hours.

3.3.2 Typical Performance Properties of Uniaxial Geogrids

Typical performance properties of uniaxial geogrids can be seen in Table 3.2

3.4 Index Tensile Testing of Biaxial Geogrids

3.4.1 Methodology and Analysis

For manufacturing quality control testing, in-plane uniaxial (CRS) testing has been used from the time of the development of the first biaxial geogrids with integral junctions. However, the test methodology and test conditions were never widely published nor widely agreed.

For specification purposes in-plane, uniaxial CRS testing of biaxial geogrids, McGown et al (1984), once again suggested using a constant rate of strain of 2% per minute and standard material conditioning test conditions of 20°C ± 2°C and 65% ± 2% humidity to establish reference load strain properties for these geogrids, with separate tests carried out in the machine and cross-machine directions.

Since this initial development work, Index properties testing standards have evolved, with the current testing standard for CE marking being ISO 10319 (2015), Typical test data are plotted as shown in Fig 3.6 to 3.7. The plots show uniaxial CRS results of Tensar SS20 tested in the machine direction

and the cross-machine direction. The Tensar SS20 MD gives a mean strength of 20.46 kN/m and a mean strain at maximum load of 9.50% and the Tensar SS20 CMD gives a mean strength of 23.17 kN/m and a mean strain at maximum load of 10.38%.

Neither National or International Standards exist for biaxial Index testing of biaxial geogrids with integral junctions. The only previous work relating to this is that carried out by Kupec (2004). He suggested that for biaxial Index testing, a cruciform shaped specimen should be used, seen in Fig 3.8. The cruciform shape, at higher strain levels, prevents distortion of the geogrid and avoids the problem associated with non-uniform stress conditions, Bridgens & Gosling (2003). The test methodology employed by Kupec (2004) was generally in accordance with BS6906 Part 1 (1987). The specimen was held in clamps which prevented slippage and specimen damage, and tested in a controlled atmosphere at 20 ± 2°C and 65% relative humidity. Two calibrated load cells, accurate to ± 0.5kN, were used to measure the loads. The same deformation rate of 1mm/min was used in the primary and secondary directions with deformations measured at the clamps using Linear Variable Differential Transformers [LVDT] and at various points on the specimen using a digital photogrammetry technique which involved a digital camera mounted above the test specimen. For these short-term CRS tests, photographs at 30 second intervals were used.

3.4.2 Typical Uniaxial and Biaxial Index Tensile Properties of Biaxial Geogrids

The Index properties for uniaxial CRS testing on a biaxial geogrid, as carried out by McGown et al (1984), can be seen in Fig 3.9. The results show that this biaxial geogrid does not possess equal properties in the machine and cross-machine directions

Later, uniaxial and biaxial CRS testing was carried out by Kupec (2004) on a biaxial geogrid with integral junctions with similar properties in the machine and cross-machine directions. The test data can be seen in Fig 3.10. These results show that the measured short-term tensile strengths of this geogrid are essentially the same in both the primary and secondary directions and

are essentially the same value, no matter if they are tested uniaxially or biaxially. However, it can be seen that the initial stiffness of the geogrid is shown to be greater when tested biaxially as the biaxially tested directions reached a point of less than 7% strain at loads of around 38 to 40 kN/m whereas the uniaxially tested directions reached strains over 8% at similar loads. This is also more evident in the detailed plots at low strains.

3.5 Performance Tensile Testing of Biaxial Geogrids

3.5.1 Methodology and Analysis

McGown et al (1984) suggested that the methodology for in-plane, uniaxial tensile Performance testing of biaxial geogrids should be essentially the same as that described in Section 3.3.1 for uniaxial geogrids, however, tests should be carried out in both the machine and cross-machine directions. The test data are plotted as shown in Figs 3.11 to 3.13. The plots show creep performance for Tensar SS20 in both the machine and cross-machine directions, tested at 30% of the ultimate strength. SS20 MD reached a strain of around 8% in around 24000 hours before it was terminated. SS20 XMD reached a strain of around 7% in the same time.

Kupec (2004) suggested that biaxial Performance tests should be carried out using the same clamping arrangements and mechanisms to those used in the biaxial CRS testing. He explained how the sustained loads are applied equally in both the machine and cross-machine directions and are applied and removed at the same time. The sustained loads are rapidly applied and removed at the end of the tests to observe the elastic strain upon loading and unloading. The sustained loads are selected as a percentage of the nominal short-term tensile strength obtained from the uniaxial CRS testing. The percentage loads applied range from 10 to 50 percent. Loads are applied for at least 100 hours and after unloading test specimens are left to recover for a further 100 hours. Testing must be carried out in a controlled atmosphere, (e.g. at 20 ± 2°C and at a relative humidity of 65%). Measurement of deformations is carried out using the same digital

photogrammetry technique as used for the CRS tests. For long-term sustained loading tests photography was undertaken on a logarithmic time scale, i.e. high frequency for the initial part of the test and a gradual lower frequency with time.

3.5.2 Typical Performance Tensile Properties of Biaxial Geogrids

The performance properties of a biaxial geogrid with integral junctions when tested uniaxially in the machine and cross-machine directions can be seen in Figs 3.14 to 3.16, Kupec (2004). Biaxial sustained loading tests carried out by Kupec (2004), can be seen in Figs. 3.17 to 3.19, Kupec (2004).

The uniaxial and biaxial, sustained load testing, data plots are combined in Figs 3.20 to 3.22 and allow direct comparisons between the two methods of testing. They indicate that the biaxially tested geogrids provide an increase in initial stiffness over uniaxially tested specimens just as in CRS Index testing. Kupec (2004) suggests that the increase in initial stiffness may be due to the combined effect of 'Poisson's Ratio' and to the re-orientation of the amorphous molecules in the junction areas of the geogrid.

3.6 Index Tensile Testing of Triaxial Geogrids

3.6.1 Methodology and Analysis

For manufacturing quality control testing, in-plane uniaxial wide-width (CRS) testing has been used from the time of the development of the first triaxial geogrids with integral junctions. However, the test methodology and test conditions were never widely published nor widely agreed.

For in-plane, uniaxial CRS testing of triaxial geogrids for specification purposes Walsh (2006) used the current wide-width testing standard for biaxial geogrids, IS0 10319 (2008), and standard material conditioning test conditions of 20°C ± 2°C and 65% ± 2% humidity to establish reference load strain properties for these geogrids. Initially tests were to be carried out in only in the primary (machine) and secondary (cross-machine) directions. However, Walsh (2006) quickly recognised that in order to properly assess this new type of geogrid it was necessary to undertake such in-plane uniaxial

wide-width tensile testing in four directions, viz. in the two ‘mid rib’ directions (0° and 60° with respect to the machine direction) and the two ‘rib’ directions (30° and 90° with respect to the machine direction). These specimen testing directions are shown in Fig 3.23.

Initially for CE marking, triaxial geogrids were treated as a new form of biaxial geogrids and the testing standard applied for CE marking was ISO 10319 (2008), see Appendix A. This meant testing in only the machine and cross-machine directions.

However, more recently, Index properties testing standards for specification purposes specifically for triaxial geogrids have been evolved. Kiwa Nederland B.V. (2012) prepared a technical report for the European Organisation for Technical Approvals (EOTA), EOTA TR41, to define testing procedures: “Non-reinforcing hexagonal geogrid for the stabilization of unbound granular layer by way of interlock with the aggregate”. This explains that the Index properties are determined according to EN ISO 10319 but differ in that the secant stiffness at low strain values is calculated, and as pointed out previously, is a better indicator of stabilisation performance. Further they point out that EN ISO 10319 was predominantly written for biaxial geogrids and that triaxial geogrids possess tensile properties in radial directions in the plane of the geogrid. The EOTA TR41 document states that accurate representation of tensile properties cannot be made by testing in just the primary [machine] direction, (0°), and secondary, [cross machine] direction, (90°). As stated previously by Walsh (2006), they state that testing must be in the ‘mid rib’ and in the ‘rib’ directions. Hence testing must be carried out in four directions consisting of two ‘mid rib’ directions (0° and 60°) and the two ‘rib’ directions (30° and 90°). These specimen testing directions are shown in Fig 3.24.

3.6.2 Index Properties of Triaxial Geogrids

The Index properties for triaxial geogrids with integral junctions carried out according to the “biaxial” wide-width testing standards applied for CE marking are only required for the 0° and 90° direction. The CE marking standards are aimed at reinforcement performance whereas the new

“triaxial” testing standard, employed by the EOTA, require the geogrids to be tested in 4 directions, as mentioned in Section 3.6.1, but are aimed at the performance of a grid in a stabilisation function. Examples of test data using these test standards are plotted as shown in Fig 3.25 to 3.28 and the properties derived from these plots are shown in Table 3.3.

3.7 Performance Tensile Testing of Triaxial Geogrids

3.7.1 Methodology and Analysis

Due to the geometry of triaxial geogrids with integral junctions, in-plane performance tensile testing would require the product to be tested in a manner similar to that undertaken by Kupec (2004) for biaxial geogrids, but with equal loading of the specimen in all the load-bearing rib directions simultaneously. Such a test has not been undertaken previously, however, development work carried out at the University of Nottingham has provided a sound basis for the establishment of both in-plane, radial, tensile testing methodologies, see later in Chapter 4.

3.8 Defects with Current Testing Methods

Current test methods have all been developed from standards that originated in the early days of the industry based on the initial products from that time. These products were predominantly uniaxial or biaxial in nature and tended to be focused on deriving maximum strain and maximum load conditions, for example, BS EN13249:2016 specifies using ISO10319:2015 to quantify strength and strain at maximum load for a geogrid for use in roads and other trafficked areas excluding asphalt reinforcement. This is acceptable for a geotextile type product using tensioned membrane as a design method, where high extension and consequently rutting is a feature, but not applicable if a stabilisation approach is adopted for a product using an interlock mechanism to minimise rutting of the sub-base

However, there are a number of factors that indicate that these methods may not be applicable to multi-axial products like TriAx® even in situations like an unpaved road with channelised traffic, the load path under a wheel is

recognised to be radial in nature not orthogonal, Tensar International Limited (2019).

Testing carried out at the Traffic Research Laboratory in the UK (TRL) and by the Dutch organisation CROW (the technology platform for transport, infrastructure, and public space) indicate that pure tensile strength is not a good indicator of performance. Tests by Jenner et al (2002), interpreted by Tensar International (2019), and CROW (2002) show this with results presented in Fig 3.29 and Fig 3.30, respectively. The CROW results have been compared with the trafficking results obtained at TRL on the same range of product classes and a good relationship was established, CROW (2002).

While it's true that stabilisation is related to the restriction of material movement, it is useful to have an in-air test that indicates radial low strain behaviour for a specific geogrid, and it is important that it is for a specific geogrid due to the many factors governing interlocking, Giroud (2009).

4. Methods and Programme of Testing TriAx® Geogrid TX160

4.1 Introduction

The TX160 geogrid used in this study is one of a range of triaxial geogrids with integral junctions. The other TriAx® geogrids in this range that possess an 80AF aperture are, TX150, TX170 and TX180. These geogrids are manufactured using the same polypropylene polymers and the same master batch package, containing carbon black, anti-oxidants and the polypropylene homopolymer carrier. The master batch package is added to the virgin polypropylene polymer at a percentage of 5.8%. The master batch addition rate tolerance should be 0% to +0.45%. The virgin polymer setting is adjusted accordingly so that the master batch and virgin polymer addition rates always total 100%.

4.2 Physical Properties

The physical properties generally used to describe geogrids are flexibility, junction type, mass per unit area, percentage open area, aperture size and shape, and overall dimensions.

According to Haliburton et al (1980), geogrids can be classed as stiff or flexible geogrids. Geogrids with a flexible stiffness ≥1000g/cm are classified as stiff and geogrids with a flexible stiffness <1000g/cm are classed as flexible. The TX160 geogrid used in this study can be classed as a stiff geogrid. This property is commonly related to the soil sub-grade strength or stiffness,

The geogrid used in the study comes from the Tensar TX range manufactured at the Blackburn factory in the UK.

The theoretical percentage open areas of TX geogrids based on geometry specifications are shown in Table 4.1.

These TX geogrids have an aperture size of (80AF) and are triangular in shape, which in-turn produces a hexagonal repeat pattern.

Tables 4.2 to 4.5 set out the basic dimensions of the TX geogrids.

The properties of the TX range of geogrids for specification purposes presently published for the testing standard (EOTA TR41:2012) specifications are shown in Tables 4.6 to 4.9. In these tables, the “Declared Values” and “Tolerances” are given. The properties according to the CE marking reinforcement specifications of the TX geogrids are shown in Tables 4.10 to 4.13.

4.3 Uniaxial Wide-Width QC, Index and Creep Test Methods

The details of these test methods are presented in Appendices A1 and A2.

4.4 Quadrant Radial Creep Test Methods

The details of this test method are presented in Appendix A3.

4.5 Test Programme

4.5.1 Q.C Testing

The Q.C testing methods adopted by Tensar International Limited are the same as those used for the Index Testing Method. Q.C test data of TriAx® are obtained by carrying out CRS wide-width testing according to ISO10319 (2015). These tests are carried out on various batches from production rolls of geogrid to obtain their short-term material properties and ensure product specifications are met. A typical batch, although this can vary, is approximately 15 tons of material with a typical batch taking 8 hours to manufacture. Therefore Q.C testing is normally undertaken every 8 hours.

The typical number of tests carried out for Q.C testing consists of five specimens tested in 0° and 90° directions and three specimens tested in the 30° and 60° directions.

Q.C test data identifies short-term material properties that are provided on the “Declaration of Performance” (DOP) of geogrids manufactured by Tensar International Limited.

Tensar adopts the principle of using process capability studies for setting product tolerances. Process capability is a long-term study, measured in Cp (Capability Process) and Cpk (Process Capability Index), that shows how well a process is performing in relation to the specification limits while the study is in progress, as well as indicating likely performance in the immediate future.

The Cp index describes process capability; it is the number of times the spread of the process fits into the tolerance width. The higher the value of Cp, the better the process. For example, if Cp = 2.5, the spread of the process fits 2.5 times into the specification width, while Cp = 1 means that the spread is equal to the specification width. This is shown in Fig 4.1.

The Cpk Index gives the position of the process in relation to the specification limits. It is not much use having a high Cp index if the process setting is way off centre in relation to the middle of the specification range.

A high Cpk index means, then, that you have a good process with a small spread in relation to the specification width, and also that it is well centred within that width. If Cpk is equal to Cp, the process is set to produce exactly in the middle of the specification range. This is shown in Fig 4.2.

Ideally, a Cpk of 1.33 or better will be targeted initially. Theoretically, this allows a shift of 1 standard deviation in the process “mean” before the lower 3 standard deviation bound of the population reaches the lower specification limit. In some cases, a Cpk of 1.00 is set as an initial target.

At a Cpk of 1.0 then 99.7% of production will be “acceptable” and 0.3% “unacceptable”

At a Cpk of 1.33 then 99.9937% of production will be “acceptable” and 0.0063% “unacceptable”

Cpk is calculated as the minimum of the 2 equations:

Mean-Lower Specification Limit (LSL) / (3σ) and Upper Specification Limit (USL)-Mean / (3σ)

So, if Mean = 100, Standard Deviation = 25, and USL = 200 and LSL = 0 (100 - 0) / (3 x 25) = 1.33, (200 - 100) / (3 x 25) = 1.33, because there are 4 standard deviations between the Mean and USL / LSL which infers the mean can drift 1 Standard Deviation up or down.

So if Mean = 100, Standard Deviation = 33.3, and USL = 200 and LSL = 0 (100 – 0) / (3 x 33.3) = 1.0, (200 -100) / (3 x 33.3) = 1.0, because there are now only 3 standard deviations between the Mean and USL / LSL (Upper Specification Limit / Lower Specification Limit), the Mean can’t drift and has to be perfectly centered.

4.5.2 Index Testing

Index testing of two different batches (Batch Ref: 056218 and 059839) was carried out using a constant rate of strain of 20% of the gauge length per minute, in four directions (0^0, 30^0, 60^0 and 90^0 with respect to the production machine direction). 5 specimens were tested per direction.

Testing rates of, 2% and 0.2% of the gauge length per minute were carried out on Batch Ref: 056218 in four directions (0^0, 30^0, 60^0 and 90^0 with respect to the production machine direction) and at 0.02% for the 0° and 90° directions.

All tests were carried out to a minimum of 3% strain.

4.5.3 Uniaxial Creep Testing

Uniaxial creep testing was carried out on Batch Ref: 056218.
Tests were carried out at 40kg, 80kg, 120kg and 160kg in four directions (0^0, 30^0, 60^0 and 90^0 with respect to the production machine direction). Multiple trial tests were carried out to perfect the set-up but only one specimen was tested per direction at each load, except for the 40kg load which was repeated in all four directions.

All tests were carried out for a minimum duration of 24 hours.

4.5.4 Quadrant Radial Creep Testing

Radial creep testing was carried out on Batch Ref: 056218.
Tests were carried out using loads of 30kg, 40kg, 50kg and 60kg per clamp in four directions (0^0, 30^0, 60^0 and 90^0 with respect to the production machine direction). Multiple trial tests were carried out to perfect the set-up.

2 tests were carried out for the 30kg, 40kg and 50kg loads. The first test was carried for a minimum duration of 10 hours with the second test being a minimum duration of 1 hour.

The 60kg test was carried out for a minimum duration of 1 hour.

5. Uniaxial Q.C, Index, and Creep Testing of TriAx® Geogrid – TX160.

5.1 Introduction

The initial testing programme of a TX160 geogrid was carried out on a single batch of TX160 geogrid (Batch Ref: 056218). This batch of TX160 was manufactured on 16/05/13 at Blackburn, but the Index testing was not carried out until 31/03/14, i.e. the "Time After Production" (TAP) was one year.

With such a long period between manufacturing and testing and knowing that certain properties can increase over time post production, it was important to investigate and identify this further.

To do this a different batch (Batch Ref: 059839) was also tested straight after production (Q.C testing) and tested later some time after production. The details and findings of this are provided later in this Chapter.

5.2. Q.C. and Index Testing

5.2.1 Q.C. Test Data

As described previously, Q.C testing is carried out in accordance with ISO10319 (2015) on samples taken straight after the manufacturing process. Q.C data for TX160 Batch Ref: 056218 had already been carried out approximately one year prior to Index testing and the data were obtained from Q.C records. The data are presented in Figs 5.1 to 5.4. TX160 Batch Ref: 059839 was Q.C tested for the purpose of this study and compared with Index test data tested 1 week after production on the same batch. This Q.C data for Batch Ref: 059839 are presented in Figs 5.5 to 5.8. Testing on both batches was carried out in four directions, 0° (MD), 30°, 60° and 90° (XMD). Five specimens were tested in 0° and 90° directions and three specimens tested in the 30° and 60°.

5.2.2 Index Test Data

In order to identify the Index properties of the TX160 geogrid, the Index testing was carried out in four directions, (0^0, 30^0, 60^0 and 90^0 with respect to the production machine direction). Figures 5.9 to 5.12 show the test results and plots from the Index testing of TX160 (Batch Ref: 056218, TAP 1 year) in the four directions, and Figures 5.13 to 5.16 show the test results and plots from the Index testing of TX160 (Batch Ref: 059839, TAP 1 Week) in the four directions, all tested in accordance to the EOTA TR41(2012). Table 5.1 and 5.2 show the mean Index properties of TX160 in the four directions, for both TX160 batches, when tested in accordance with the EOTA TR41(2012).

5.2.3 Comparison of QC and Index Test Data

It is well documented that the mechanical properties of semi-crystalline polymers, such as polypropylene, can increase due to continued crystallisation after production. This is called “Secondary Crystallisation”. Secondary crystallisation can occur for several days, even weeks, after processing. As long as the polymer temperature is above the glass transition temperature (T_g), slow crystallisation can occur after the main solidification process is complete. Since the T_g of polypropylene is around -20°C, then even at room temperature the polymer molecules will contain enough energy for the chain to move and continue the crystallisation process until it is fully complete, Cowie (1973), ASM (1988). Ehrenstein (2001) Young & Lovell (2011).

To check that this occurs as part of the production of TriAx® Geogrids, Q.C. test data were obtained for the Control Batch Ref: 056218, which was tested straight off the production line on 16/05/13. The polar plot shown in Fig 5.17 shows the comparison of secant stiffness at 0.5% for the Q.C. data and a Time After Production (TAP) of 1 year and the polar plot shown as Fig 5.18, shows the comparison of secant stiffness at 2% for Q.C. and TAP of 1 year. Tables 5.3 to 5.6 show the mean test data for all four directions straight after production and TAP 1 year.

From the above results, even though the sample tested after 1 year gave an increase in secant stiffness at 0.5%, the 60° testing direction gave a lower percentage difference value than the other 3 directions. This could be due to the differences in accuracy in the load cells used in testing for QC and the later index testing. The QC test results were generated by testing 3 specimens in the 30° and 60° directions and 5 in the 0° and 90° directions using a 100kN load cell. The index tests were carried out on 5 test specimens per direction and using a 10kN load cell, hence the accuracy levels of the two sets of test data are likely to be different.

Another reason could be due to sample selection. Samples selected closer to the edge of a roll of a TriAx geogrid, have more chance of containing a buckled/kinked rib(s). Samples are selected randomly across the roll of a grid, and even though care is taken, it is possible a sample could be selected with one or more of these buckled/kinked ribs which would affect the results.

Overall, the results indicate that both the 0.5% and 2% secant stiffness values increase over time.

To check the above data another set of tests were carried out on a different batch of TX160 (Batch Ref: 059839). The new batch was tested straight after production and again 1 week later on the same machine, using 5 test specimens per direction and a 10kN load cell. The results are presented as per Batch Ref: 056218 in Figs 5.19 and 5.22. These show the secant stiffness at 0.5% and 2% for Q.C and TAP of 1 week.

Once again, the polar plots in Fig 5.19 and Fig 5.20 show that over time the secant stiffness at 0.5% and 2% properties have increased. Tables 5.7 to 5.10 show the mean test data for all four directions straight after production and TAP 1 week.

The above results confirm that the secant stiffness values at 0.5% and 2% of TX160 increase with increasing TAP.

The test results for Batch Ref: 059839 were much more uniform than the data for Batch Ref: 056218. This was probably due to the testing conditions

being the same for the samples of Batch Ref: 059839 when tested straight after production and after 1 week.

Overall the results confirm the previous testing for Batch Ref: 056218 and show that both the 0.5% and 2% secant stiffness values increase over time after production.

5.2.4 Comparison of QC and Index Test Data to Declared Values

In addition to comparing the properties of specimens tested some time after production, and Q.C test properties obtained straight after production, these properties were compared against product specifications and in accordance with the EOTA TR041:2012. The declared values of secant stiffness at 0.5% and 2%, for TX160, are 390kN/m (-75kN/m tolerance) and 290kN/m (-65kN/m tolerance) respectively.

Figures 5.21 to 5.24 show polar plots of all these tests, compared with their declared values and tolerances. With no upper tolerance declared in the EOTA TR041:20112, the upper tolerance value was chosen as +75kN/m for 0.5% secant stiffness and +65kN/m for 2% secant stiffness.

Overall the results show that all the QC test data and the TAP test data conform to the EOTA TR041:2012 product specifications.

By carrying out these tests on two different batches of TX160, it has been shown that secondary crystallisation does take place and that it influences the test results obtained. Indeed, the test data shows that over a period of at least 7 days, the secant stiffness values increase significantly when compared to tests carried out straight after production for QC purposes.

The tensile results from both batches show the 90° direction has the highest secant stiffness values.

Comparing the results against the EOTA TR041:2012 specifications has shown that, for both batches, subject to QC testing and Index testing some time after production, the secant stiffness values in all four directions are above the declared values.

The test results show that the “Secant Stiffness Ratio” decreases somewhat after time. Batch 056218 shows a decrease from 0.88 to 0.84 and Batch 059839 shows a decrease from 0.86 to 0.81. Even though a decrease occurs the ratio is still well within the range specified in EOTA TR041:2012, which declares a secant stiffness ratio, for TX160, for secant stiffness at 0.5% as 0.80 with a tolerance of -0.15.

5.2.5 The Relationships Between Secant Stiffness, Maximum Load and Strain at Maximum Load.

To check if there were simple correlations between the 0.5% and 2% secant stiffness values and the maximum loads and the strains at maximum loads, Figs 5.25 to 5.28 were plotted for the QC and TAP test data for TX160, for Batches Ref: 056218 and 059839.

These plots show that there are no simple consistent correlations between the secant stiffness and maximum loads and strains at maximum loads. Thus, it is necessary to establish directly the secant stiffness values.

5.2.6 Influence of Strain Rates

Figs 5.29 to 5.32 show the load/m vs strain plots of TX160, Batch Ref: 056218, CRS test data, for testing 1 year after production at strain rates of 20%, 2%, 0.2% and 0.02% of the gauge length per minute. (The gauge length is determined as in the EOTA TR041:2012). From these plots it shows that testing at gradually slower strain rates results in a reduction of load/m.

Figures 5.33 and 5.34 show polar plots of TX160, Batch Ref: 056218, CRS test data, for testing 1 year after production at strain rates of 20%, 2%, 0.2% and 0.02% of the gauge length per minute. (The gauge length is determined as in the EOTA TR041:2012). Testing at gradually slower strain rates shows that the secant stiffness values at 0.5% and 2% strain reduce with reduction in strain rate. Tables 5.11, 5.12 and 5.13 shows the mean data for all the four directions of index properties tested at a constant rate of strain of 2%, 0.2% and 0.02% of the gauge length

Overall the index properties reduce as the testing strain rate is lowered and the 90° direction remains the direction with the highest secant stiffness values. Testing at lower strain rates had little effect on the secant stiffness ratio. Testing at 20%, 2%, 0.2% and 0.02% constant rates of strain, gave secant stiffness ratios between 0.85 and 0.78 respectively.

Figures 5.35 and 5.36 show the secant stiffness at 0.5% and 2% versus log time for TX160 tested at constant rates of strain of 20%, 2%, 0.2% and 0.02%.

5.3 Uniaxial Creep Testing

5.3.1 Introduction.

Sustained load (creep) testing of geosynthetics has been widely studied and the influence of time and temperature on their behaviour clearly identified, Kabir (1984), McGown et al (1984), Yeo (1985), and Wrigley et al (1999). To a lesser extent, the behaviour of geosynthetics under sustained strain, stress relaxation testing has been studied and the influence of time and temperature similarly identified, Soong et al (1994). As well as the above, cyclic testing has also been investigated by Müller-Rochholz et al (1994), Khan (1999) and Kanyoza (2003). Significantly, all the data obtained produce different load-strain-time-temperature responses even for a particular geosynthetic product type.

The above test methodologies involve different forms of data presentation and for some particular tests several forms of data presentation can be used. With regards to creep testing the data can be presented in number of ways, these are shown in Fig 5.37 ASM (1988). The method of data presentation for the TX160 geogrid is that used to plot the creep test data for uniaxial and biaxial geogrids, McGown et al (1984).

5.3.2 Uniaxial Creep Test Data

Figures 5.38 to 5.45 show the creep strain plots from the performance testing of TX160 Batch Ref: 056218, for four different loads, 40, 80, 120 and 160 Kg, in four directions, 0^0, 30^0, 60^0 and 90^o with respect to the production machine direction. The loads used for these tests were the same set loads for each direction.

The test data are presented as isochronous load-strain curves at a constant temperature. Commonly these are produced from creep test data, Fig. 5.46, however, they can also be produced from most test procedures, e.g. a series of CRS tests at different strain rates, Fig. 5.47.

Figures 5.48 to 5.52 show the isochronous load-strain plots derived from the TX160, Batch Ref: 056218, creep test data. The load (kN/m) was calculated from the theoretical widths outlined in the EOTA TR041:2012. These isochronous plots contain upper and lower boundaries of the data set.

5.3.3 Analysis of Creep Test Data

The strain-time creep curves for all four loads shows that the 90° direction produces the lowest strain out of the four directions tested. This is shown in both the initial loading (first 10 seconds) and overall strain curves.

The 30° direction consistently produces the highest initial strain (strain in the first 10 seconds) when tested at all four loads. It also gives the highest overall strain when tested at 40kg and 80kg but similar overall strain to the 0° direction when tested at loads of 120kg and 160kg.

Using the data in Figures 5.48 to 5.52, a fitted smooth data curve was taken through the upper and lower limits of the data. From these load-strain time curves a 0.5% isochronous load versus time graph, Fig 5.53, and an isochronous stiffness at 0.5% versus time graph, Fig 5.54, was created using the line of best fit data.

Fig 5.54 shows that over time stiffness in all four directions decreases. The 90° direction of TX160, when tested under sustained load, has a much higher stiffness than the other 3 directions. The 0°, 30° and 60° directions

behave very similarly with the stiffness in the 60° direction decreasing more slowly over time.

5.4 Comparison of Creep and CRS Test Data

It was established that, for CRS testing, there was no simple consistent correlation between the secant stiffness and maximum loads and strains at maximum loads and that it is necessary to establish directly the secant stiffness values. With no specifications and very little data available for sustained loading tests the same principle of establishing the secant stiffness values was used. This allows for a more comparable data set.

Fig 5.55 shows the best fit data sets of 0.5% secant stiffness for both CRS and creep testing.

Both sets of data indicate that the grid exhibits the same behaviour when tested either by creep or CRS with regards to the 90° direction being the stiffest and the 0°, 30° and 60° directions behaving very similarly, with the stiffness values of the 60° direction decreasing at a slower rate.

Fig 5.55 shows that uniaxial creep testing gives a higher initial secant stiffness than when testing by mean of CRS. This is down to the uniaxial creep test undergoing a pure elastic response upon applying the load hence an instantaneous high load with visco-elastic behaviour initiating over time. With CRS testing elastic and visco-elastic behaviour occurs inseparably as the load is applied much more slowly and gradually.

The stiffness of both test methods is shown to decrease over time but at different rates. The stiffness in a creep test decreases a lot quicker than when tested using CRS.

Though the geogrid behaves differently for the two testing methods eventually the data lines cross, indicating that the data from either method at a certain point can be used. The 0°, 30° and 60° directions data points cross between 2-4 hours, whereas the 90° direction data points cross at approximately 30 hours.

5.5 Discussion

Details of uniaxial CRS and uniaxial Creep data were presented. It was established that time after production (TAP) can have a significant effect on the material properties, more accurately, mechanical properties increase with time which confirms that some form of secondary crystallisation takes place. Comparing results after this secondary crystallisation takes place to the Q.C testing that occurs straight off the production line, it can be concluded that the current Index property specifications of TX160 could be conservative as these specifications are established from Q.C test data and not from products that have undergone significant secondary crystallisation.

Testing was carried out on identical test specimen shapes and from the same production batch. Secant stiffness values obtained from both CRS and creep testing were compared against each other. This comparison showed that the geogrids tested exhibit very similar behaviour when tested either by creep or by CRS. These tests indicate that the 90° direction is the stiffest direction with the other directions behaving similarly.

6. Quadrant Radial Creep Testing of TriAx® Geogrid – TX160

6.1 Background

In Chapter 3, Section 3.7, it was identified that no “in-plane” performance or performance related tensile testing had been undertaken previously. This Chapter focuses on the development of a new in-plane performance related testing apparatus capable of testing TriAx® geogrids radially and providing radial load-strain properties.

Radial “out-of-plane” testing such as the plunger and dome burst tests were considered but they involve large out-of-plane deformations. Also, they are difficult to initialise, to interpret and it is difficult to compare test data to that obtained from standard testing.

To achieve this a new outward radial in-plane creep testing apparatus was developed to carry out a radial creep testing programme. This was chosen as it is not difficult to initialise, does not involve large deformations, and test data can be easily interpreted and compared to that obtained from standard testing.

The geogrid to be tested was TriAx TX160 geogrid (Batch Ref: 056218), Figures 6.1 to 6.3 show this apparatus and the test methodology is described in detail in Appendix A3.

6.2 Quadrant Radial Creep Testing

6.2.1 Introduction

In Chapter 3, tensile testing of uniaxial and biaxial geogrids was described in detail. For uniaxial geogrids, uniaxial tensile testing was shown to be appropriate for their reinforcement function in one direction and relatively narrow uniaxial test specimens are considered to be representative, McGown et al (1984).

For biaxial geogrids, biaxial tensile testing was shown to be appropriate for their biaxial reinforcement function and cruciform test specimens were tested, Kupec (2004). However, uniaxial wide-width tensile tests are generally still carried out in the MD and XMD directions, Kupec (2004). This uniaxial wide-width tensile testing provides an underestimate of the material stiffness, but the relative simplicity of undertaking these uniaxial wide-width tests means that they are adopted as standard, e.g. EOTA TR041(2012), ISO 10319 (2015).

Unlike biaxial geogrids, which have two sets of ribs at right angles to each other (i.e. one in the MD direction and one in the XMD direction). TriAx® geogrids have three sets of ribs that are oriented at 30°, 60°, and 90° to the MD.

When testing TriAx® geogrids uniaxially, the ribs that strain, although not necessarily in an equal manner, depend on which direction the geogrid is loaded. Figures 6.4 to 6.7 show the main direction of loads and strains in the ribs when TriAx® geogrids are tested in specific uniaxial directions.

For radial testing there will be two principal directions of loading/strains, the radial direction and the circumferential direction. Figures 6.8 to Fig 6.11 show the radial and circumferential directions in relation to the direction of testing. Although the circumferential and radial directions change, the loads/strains in the rib are always axial, however, the loads/strains in the junctions will develop different loads and strains depending on their relative orientation to the direction of testing. The junctions may therefore be stretched in an asymmetric manner.

For TriAx® geogrids, an outward radial test consisting of a large diameter circular shaped test specimen would be the most appropriate method of testing. However, carrying out such a test would provide many practical difficulties related to clamping and uniformity of loading. Therefore, it is likely that uniaxial tensile tests on wide width test specimens will generally be carried out in multiple directions as is the case for Index testing as stipulated in the EOTA (2012) and described in Chapter 3, Section 3.6. Nevertheless, it will be necessary to establish whether or not the stiffness data obtained by

multi-directional uniaxial tensile testing of wide width test specimens provides an underestimate or overestimate of the performance related radial stiffness of TriAx TX160 geogrids.

In order to establish the above, one or more 30° segments of a circular test specimen should be tested. For TriAx TX160 geogrids a circular test specimen may be divided up into twelve 30° segments. Testing a single 30° segment would problematic due to the lack of any edge restraint. This would lead to “necking” of the test specimen during straining. To avoid, or at least minimise this effect multiple segments need to be tested. Following a preliminary testing programme, it was decided to test three 30° segments with the addition of edge restraints. This is the so-called “quadrant” shaped test specimen and the two forms of these which are tested are shown in Figures 6.12 to 6.15.

The other size factor that needs to be taken into account is the radial dimension of the quadrant shaped test specimen. In terms of practicality of clamping, the minimum width of the inner clamp requires to be greater than the distance across the points of the basic hexagonal structural unit of the TriAx geogrid. Thus, the width of the inner clamp must be at least 100mm for a TriAx TX160 geogrid, giving an inner radius of some 190mm. In order to determine the strain gradient with increasing radius, a representative number of basic hexagonal structural units requires to be included in the test specimen. It was decided that a minimum of four units should be included, thus the outer radius should be at least 550mm and the outer clamp for each three 30° segment would then be some 300mm wide. Thus, the suggested shapes and sizes of the quadrant test specimens are shown in Figures 6.16 and 6.17.

All the tests were carried out at an ambient temperature of 20°C ± 2°C

6.2.2 Variation of Loads and Strains within Radial Test Specimens

Edge restraints are added to the test rig to prevent any radial or circumferential distortion and to allow an even distribution of loads throughout the test specimen. To ensure that these conditions were

maintained throughout the tests, detailed measurements and analysis of photos were taken and examples are shown in Plates 6.1 to 6.6. Plate 6.1 shows the test specimen before load is applied. Plates 6.2 to 6.6 show the test specimen under load at approximately 30 seconds, 1 minute, 5 minutes, 1 hour and 72 hours after loading. All plates show the test arrangement for 30° and 90° testing direction. Detailed analysis of these photographs was undertaken, and it was shown the specimen deformations are very uniform and that there are no signs of buckling of the ribs during and right up to the end of the tests. Thus, it may be stated that the test set-up using edge restraints allows the samples to perform in a consistent radial load/strain manner and that all test will be performed using edge restraints.

On the basis of the above, it may be expected that with radial testing of quadrant test specimens with edge restraints, the applied load/m and the strains that occur upon loading vary with distance along the radius of the test specimen and both radial and circumferential (hoop) loads and strains are developed. The ribs are essentially subject to tensile loads and the integral junctions are subject to biaxial loads and a degree of torsional loading.

Knowing the applied load/m at the outer clamps, the applied load/m at any point along the radius can be calculated.

Further, knowing the overall Radial Gauge Length and the Overall Deformations, the Average Radial Strains and the variation of radial strain along the (radial gauge) length can be calculated.

Figures 6.18 to 6.19 show examples, based on the 3x30kg applied load radial creep test at the outer radius (30kg on each outer clamp), of the calculations used to determine the applied load/m at the outer clamps (R560 and R550), the average load/m over the gauge length and the radius at this average load/m for the 0°/60° and 30°/90° directions of testing

Using the aforementioned calculations, the applied load/m at the outer clamps, average load/m over the gauge length and the radius at this average load/m were all calculated for each direction of testing and are shown in Table 6.1.

With the applied load/m at the outer clamps known, the local average load/m at each radii (node) can be calculated, and with the average load/m over the gauge length known and the strain at a specific time interval e.g. 0.001 hours the radial tensile stiffness (kN/m) can also be calculated which in turn allows for local average strains to be calculated at specific time intervals. All the above data for each load and direction are shown in Tables 6.2 to 6.17 with the plots shown in Figures 6.20 to 6.35.

6.2.3 Quadrant Radial Creep Test Data

Quadrant radial creep testing was carried out on the same batch (Batch Ref: 0562180) of TriAx TX160 as used for the CRS and uniaxial creep testing programmes.

Figures 6.36 to 6.39 show the creep strain plots from radial testing TriAx TX160 for 4 different applied loads to the outer clamps, 3x30kg, 3x40kg, 3x50kg and 3x60kg (all loads are applied to each outer clamp, hence 3x the load), in four directions, 0°, 30°, 60° and 90° with respect to the production machine direction. The loads used were the same loads for each direction.

The applied average load (kN/m) was calculated using the calculations set out in section 6.2.2 with the data shown in Figures 6.40 to 6.44. These isochronous plots contain a fitted smooth data curve plotted through the upper and lower boundaries of the data set and shows the 0.5% Secant Stiffness values.

6.2.4 Analysis of Creep Test Data

Using the isochronous average load-strain time curves, Figures 6.40 to 6.44, and calculating average load/m, comparable behaviours in the four directions are obtained. On these plots, a fitted smooth data curve was taken through the upper and lower limits of the data.

The plots also contain a dashed blue line from 0.5% strain passing through zero. This data line is used for calculating the secant stiffness at 0.5% strain.

From these load-strain time curves a 0.5% average load/m versus time graph, Fig 6.45, and an isochronous stiffness at 0.5% versus time graph, Fig 6.46, was created using the upper and lower boundaries.

6.3 Discussion

Preliminary testing indicated that edge restraints are necessary for the radial test to perform in a radial load/strain manner.

Details of quadrant radial creep test data were presented. Table 6.1 presents the calculations of Applied Load/m at Outer Clamps, Average Load/m Over Gauge Length and Radius at Average Load/m for all radial test specimens tested at 0°, 30°, 60° and 90° directions at four different loads. These calculations show that the radius at average load/m is 318mm for 0° and 60° directions and 270mm for 30° and 90° directions. The applied load/m at the outer clamps and the average load/m over gauge length are greater for 30° and 90° directions than 0° and 60° directions.

The radial creep testing was carried out on the same TriAx TX160 batch as the CRS and uniaxial creep tests. The plotted isochronous secant stiffness presented in Fig 6.46, indicates that the stiffness decreases with time.

Chapter 7: Low Strain Behaviour of TriAx® Geogrid – TX160

7.1 Introduction

The critical properties of multi-axial geogrids in the stabilisation of unbound pavements have been identified by Giroud (2009) and Giroud and Han (2016) as their short-term, low-strain, radial tensile stiffness and their interlock characteristics. The interlock characteristics of stiff geogrids have been widely investigated and are well understood, but this is not the case for their short-term, low-strain, radial tensile stiffness.

For the purposes of awarding European Technical Approval for multi-axial geogrids in sub-grade stabilisation, EOTA (2012) adopted the methodology of in-plane, wide-width uniaxial testing in multiple directions in order to determine the short-term, low-strain radial tensile stiffness of the geogrids, however, the validity of this testing approach required to be confirmed. Therefore, the new in-plane, radial, tensile radial test method was developed employing 90^0 segment shaped test specimens

With the short-term, low-strain, radial tensile load-strain behaviour of geogrids being less established, three different methods of testing the TriAx multi-axial geogrids have now been undertaken (CRS, uniaxial creep, and radial creep) to characterise this behaviour.

7.2 CRS, Uniaxial Creep, and Radial Creep Behaviour

The Isochronous secant stiffness at 0.5% strain test data obtained from CRS, uniaxial creep and radial creep test methodologies has been plotted together and shown in Fig 7.1. The plot presents the upper and lower boundaries of the Secant Stiffness at 0.5% Strain vs Log Time data for all three test methodologies.

The test data from the three test methodologies were plotted individually against each other, uniaxial creep against radial creep, uniaxial CRS against

uniaxial creep and uniaxial CRS against radial creep. These data are presented in Figures 7.2 to 7.4 respectively.

Using the test data obtained, stiffness ratios were calculated and plotted. Fig 7.5 shows the comparison, of the upper and lower data boundaries, of the stiffness ratios between uniaxial creep-to-radial creep, and uniaxial CRS-to-radial creep.

The data in Fig 7.5 shows that the difference in upper and lower stiffness ratios of uniaxial creep to radial creep is bigger than the stiffness ratio of uniaxial CRS to radial creep and shows that over time the stiffness ratios of uniaxial creep to radial creep decreases at a much quicker rate than the stiffness ratio of uniaxial CRS to radial creep with the difference between the lower and upper ratios getting continuously bigger. At times greater than half an hour the lower stiffness ratio is closer to 1. The upper and lower stiffness ratios of uniaxial CRS to radial creep remain much closer together though are not close to 1.

7.3 Locked-in Stress

Closer inspection of the above test data indicates that there may be a “locked-in stress” within the product. This locked-in stress, also referred to as “residual stress” can be defined as the stress that remains in a body at rest, in equilibrium, at uniform temperature, when all applied stresses have been removed, ASM (1988). These stresses can occur by several means with examples being flow-induced, thermal-induced and process-induced stresses, Withers and Bhadeshia (2001).

Figures 7.6 to 7.19 show the plots of uniaxial CRS data, uniaxial creep data, and radial creep data using best fit upper and lower boundary lines passing through the locked-in stress of 1kN/m at zero strain. However, it should be noted that the test data shows that it takes a strain of some 0.5% to “take-up” this locked-in stress. Thus, there appears to be a locked-in stress of approximately 1kN/m.

Figures 7.6 to 7.19 also contain a dashed blue line from 0.5% strain passing through zero. This data line is used for calculating the secant stiffness at 0.5% strain without a locked-in stress.

Fig 7.20 presents the upper and lower boundaries of the Secant Stiffness at 0.5% Strain vs Log Time data for all three test methodologies assuming a locked-in stress of 1kN/m.

Fig 7.21 shows the comparison, of the upper and lower data boundaries, of the stiffness ratios between uniaxial creep-to-radial creep, and uniaxial CRS-to-radial creep when assuming a 1kN/m locked-in stress.

Fig 7.22 shows the comparison of stiffness ratios with and without the assumption of a 1kN/m locked-in stress.

Table 7.1 presents the upper and lower gradient values of CRS, radial creep, and uniaxial creep testing with and without an assumed locked-in stress.

CRS and uniaxial creep testing show data points between 0 and 0.5% strain that are slightly off trend of the assumed 1kN/m locked-in stress. This is probably due to the sensitivity of the test/measurement in that range. Although the data, in particular for uniaxial creep testing, does not sit exactly on the assumed locked-in stress boundary line it is close to the area that the data would expect to fit.

7.4 Discussion

Comparisons of uniaxial CRS, uniaxial creep and radial creep data were presented. All three test methodologies produce different stiffness values but they all follow the same trend in that stiffness decreases with time but at different rates.

Closer examination of load/m vs strain data of all three test methodologies indicates that a locked-in stress of around 1kN/m is possibly present within the product which is most likely due to the manufacturing process and is a

result of the material obtaining equilibrium after it has undergone plastic deformation, in this case stretching.

Replotting stiffness values using the locked-in stress data makes the results more comparable.

Table 7.1 presents the gradients of the upper and lower boundaries of both the locked-in stress and no locked-in stress. The data shows that using the locked-in stress data brings the gradients of all three test methodologies closer together. The uniaxial creep gradients are still much bigger than the CRS and radial creep, but the CRS and radial creep gradients become very similar and indicate that stiffness decreases at the same rate for both of these test methodologies. This is backed up by the stiffness ratio values presented in Fig 7.22.

Fig 7.22 also shows that the locked-in stress of 1kN/m also brings the stiffness ratios of uniaxial CRS to radial creep much closer to one and for longer durations when compared to data without a locked-in stress of 1kN/m.

Both uniaxial CRS and radial Creep testing was undertaken on a single batch of TriAx® TX160 geogrid and the in-plane, radial secant stiffnesses at 0.5 per cent strains over relatively short time periods of up to 10 hours were obtained. It was found that there was a close correlation between these data. Thus, the multi-directional, uniaxial CRS tensile test was shown to be a reasonable and conservative means of determining the short-term, low-strain, radial tensile stiffness of multi-axial geogrids and the need for more elaborate testing methodologies is not required.

8. Summary, Discussion and Conclusions

8.1 Summary

In Chapter One, the geogrid TriAx® was defined along with its intended uses and applications. The term “Stabilisation” was described along with the objective of the study, which is to link the the radial, short term, low strain stiffness to the uniaxial, short term, low strain stiffness, in order to determine if a simple uniaxial testing method can be employed in the future to characterise the radial, load-strain behavior of triaxial geogrids used in stabilisation applications. The thesis layout was included at the end of this Chapter.

In Chapter Two, the development of geogrids with integral junctions was described. It explains how Dr. Brian Mercer invented the first extruded polymer mesh process and how he went on to research and develop the oriented polymer products from uni-planar starting material by punching a pattern of holes in extruded sheet, heating the material and then stretching it, paving the way for uniaxial and biaxial geogrids.

Development of uniaxial and biaxial products continued until a completely new step change in the manufacturing of geogrids with integral junctions occurred.

This came from Mr. Anthony Walsh’s idea of incorporating a 45° angled rib within a square grid aperture creating a third direction of properties to be defined. This created a geogrid with triangular apertures and in-turn produced a hexagonal repeat pattern within the geogrids. This new type of geogrid was classed as a “Triaxial Geogrid” and given the name TriAx®.

In Chapter Three, the tensile testing of geogrids with integral junctions were introduced. Methodology and analysis of Index and Performance testing of Uniaxial, Biaxial and Triaxial geogrids were described. Defects of current testing methods are identified.

In Chapter Four, the physical properties of TX geogrids were presented along with the methods and programme of testing TriAx® TX160 geogrids and the Q.C. Testing, Index Testing, Uniaxial Creep Testing, and Quadrant Radial Creep Testing described.

In Chapter Five, the Q.C Testing and Index Testing data were presented, and the data compared. Comparison of Index and Q.C. data to declared values were also presented.

Testing at different strain rates was carried out and the influence it as on the secant stiffness values were analysed.

Uniaxial Creep test data and analysis were presented and compared against CRS data.

In Chapter Six, Quadrant Radial Creep Testing was described and identified how the specimen dimensions were chosen. It was found that the test specimens needed to be restrained laterally for it to behave in a true radial manner and this was proven by undertaking detailed photogrammetry. Photographs were taken at certain intervals and analysed in detail to ensure no radial or circumferential distortion occurred.

The variation of loads and strains within radial test specimens was reviewed. Knowing the applied load/m at the outer clamps, the applied load/m at any point along the radius could be calculated. The applied load/m at the outer clamps, average load/m over the gauge length and the radius at this average load/m were all calculated and presented in this Chapter.

All Quadrant Radial Creep test data and analysis was presented in this Chapter.

In Chapter Seven, the low strain behaviour of TriAx TX160 geogrid was reviewed. Test data from all three test methodologies, CRS, Uniaxial Creep, and Quadrant Radial Creep, was compared.

Analysis of the data revealed that there was plausible “locked-in” stress present within the geogrid as a result of the manufacturing process. Locked-

in stress data was presented for all three test methodologies and compared with the no locked-in stress data.

8.2 Discussion

In Chapter Five, test results from Q.C. test data of 2 different batches and Index test data from the same two batches but with different TAP times were presented. The two different TAP times were 1 year (Batch 056218) and 1 week (Batch 059839). The two different TAP times were used to indicate that a secondary crystallisation process occurs after production and in turn increases mechanical properties. The Q.C. data and TAP data were compared against the production specification and it was concluded that the Q.C data used in specifications were conservative.

Further testing was carried out to investigate the influence of strain rates. CRS testing was carried out on the TAP 1 year batch and concluded that load/m and secant stiffness properties reduce as the strain rate reduces.

Test results from Uniaxial Creep test data (Batch 056218) was presented and compared against the CRS data. Both Creep and CRS data indicates that 90° direction is the stiffest direction and the 0°, 30° and 60° directions behave very similarly. Uniaxial creep testing gives a higher initial secant stiffness compared to CRS testing. This is due to the uniaxial creep test undergoing an elastic response upon applying the load hence an instantaneous high load with visco-elastic behaviour initiating over time. With CRS testing elastic and visco-elastic behaviour occurs inseparably as the load is applied much more slowly and gradually.

In Chapter Six, preliminary Quadrant Radial Creep testing indicated that edge restraints are necessary to prevent any distortion or buckling and for the radial test to perform in a true radial load/strain manner.

Quadrant radial creep test results from the same batch used for CRS and Uniaxial Creep (Batch 056218) were presented along with calculations and results of Applied Load/m at Outer Clamps, Average Load/m Over Gauge Length and Radius at Average Load/m for all radial test specimens tested at 0°, 30°, 60° and 90° directions at four different loads. This data showed that

the radius at average load/m is 318mm for 0° and 60° directions and 270mm for 30° and 90° directions. The applied load/m at the outer clamps and the average load/m over gauge length are greater for 30° and 90° directions than 0° and 60° directions.

Isochronous secant stiffness was plotted as per the other test methodologies producing the same behaviour, that stiffness decreases with time.

In Chapter Seven, the results of low strain behaviour of TriAx® TX160 obtained from CRS testing, Uniaxial Creep testing, and Quadrant Radial Creep testing were all collated, compared, and presented. They all produce different stiffness values, but they all indicate that stiffness decreases with time but at different rates.

Using the test data obtained, stiffness ratios were presented with upper and lower data boundaries of the stiffness ratios between uniaxial creep-to-radial creep, and uniaxial CRS-to-radial creep. The data indicates that the stiffness ratio of uniaxial creep to radial creep is greater than the stiffness ratio of uniaxial CRS to radial creep but decreases at a much quicker rate. At times greater than half an hour the lower stiffness ratio of uniaxial creep to radial creep is closer to 1 but continues to decrease over time. The stiffness ratio of uniaxial CRS to radial creep are much closer together with the stiffness ratio decreasing at a much slower rate but are not close to 1.

Further analysis of the load/m vs strain data of all three test methodologies shows that a locked-in stress of around 1kN/m is possibly present within the product, which is most likely due to the manufacturing process and is a result of the material obtaining equilibrium after it has undergone plastic deformation, in this case stretching. Using this locked-in stress data and replotting the stiffness values makes the results more comparable.

The in-plane, radial secant stiffnesses at 0.5 per cent strains obtained indicated that there was a close correlation between these data and therefore the multi-directional, uniaxial CRS tensile test was shown to be a reasonable and conservative means of determining the short-term, low-strain, radial

tensile stiffness of multi-axial geogrids and the need for more elaborate testing methodologies is not required.

8.3 Conclusions

The conclusions from the present study are:

- Comparing secant stiffness obtained from three different test methodologies, uniaxial CRS testing, uniaxial creep testing and quadrant radial creep testing, shows that there is a close correlation between uniaxial CRS and quadrant radial creep testing. A comparison of the isochronous secant stiffness data from these uniaxial CRS tests and the radial creep tests shows them to be closely and consistently related. The CRS testing does provide lower stiffness values then the quadrant radial creep test and therefore can safely say that the radial secant stiffness of TriAx® TX160 characterised in the ETA are conservative. Thus, the use of multi-directional, uniaxial CRS testing has been shown to be an appropriate test methodology for the specification of TriAx® geogrids and more complex test methodologies are not required for this product range.

- A new test rig was designed and developed to allow for multi-axial in-plane testing of TriAx® geogrids. A new test methodology of In-plane Quadrant Radial Creep testing of TriAx® geogrids was also developed.

- Radial Creep tests of TriAx® TX160 geogrids were successfully carried out using the new, in-plane radial test apparatus.

- TAP (time after production) has a significant effect on the properties of a TriAx® TX160 geogrid even after the short period of time of a week. Current Index property specifications of TX160 could be deemed conservative as these specifications are established from Q.C test data determined form products taken straight off the production line

and not from products that have undergone the significant secondary crystallisation that occurs over time that results in the increased Index property values.

- Studying the data obtained from the uniaxial CRS, uniaxial creep, and radial creep test methodologies shows that there is a possible locked-in stress of around 1kN/m. Re-plotting the data using this locked-in stress allows for more comparable data.

- All testing and data obtained in this study was carried out on TriAx® TX160 geogrids only. In-plane radial testing of other different multi-axial type geogrids will need to be conducted in order to obtain their necessary values.

- Lateral restraint of a TX160 geogrid is important to achieve a test that performs in a radial manner and is a factor other testers should take into account when testing geogrids radially.

- Not all materials perform in a way that orthogonal behaviour and properties are important. This is an important factor for other testers to consider when testing geosynthetics.

Recommendations for Future Research

- The work carried out in this thesis recognised that there was possibly a locked-in stress present within the TriAx® TX160 geogrid. It is suggested that this locked-in stress, how it is achieved, how it can be increased and how it has an effect on properties, should be investigated.

- It is suggested that radial CRS testing should be investigated and compared with the results obtained in this study.

- It is suggested that cyclic radial loading should be investigated to see how the radial loading and unloading has an effect of the properties of a TriAx TX160 geogrid.

- It is suggested that single rib CRS testing of TriAx TX160 geogrid in the -30°, +30° and XMD should be investigated and compared with the wide-width CRS testing.

- It is suggested that the work carried out in this study should be carried out for other non-TriAx®, multi-axial type, geogrids.

REFERENCES

ASM (1988) *Engineering plastics. Vol 2. Ohio, USA.*

ASTM D6637-11 (2012) *Standard test method for determining tensile properties of geogrids by the single or multi-rib tensile method.*

Bridgens, B.N. and Gosling, P.D. (2003) *Biaxial fabric testing to determine in-situ material properties.* Proceedings of the International Conference on Structural Membranes, 2003. Barcelona, Spain.

BS 6906-Part 1 (1987) *Methods of test for geotextiles. Determination of the tensile properties using a wide width strip.*

BS 6906-Part 5 (1987) *Methods of test for geotextiles. Determination of creep*

BS EN 13249:2016 *Geotextiles and geotextile-related products. Characteristics required for use in the construction of roads and other trafficked areas (excluding railways and asphalt inclusion).*

BS EN 13250:2016 *Geotextiles and geotextile-related products. Characteristics required for use in the construction of railways.*

BS EN ISO 13431 (1999). Geotextiles and geotextile-related products - Determination of tensile creep and creep rupture behaviour. International Standard Organisation. Switzerland.

BS EN ISO 10319 (2015). *Geotextiles - Wide-width tensile test. International Standard Organisation. Switzerland.*

BS EN ISO 10318-1:2015+A1:2018 Geosynthetics. Terms and definitions

Cowie, J.M.G. (1973) *Polymers: chemistry & physics of modern materials.* Aylesbury, Bucks: International Text Book Company Limited.

CROW Publicatie 157 (2002) *Dunne asfaltverhardingen: dimensionering en herontwerp.*

Ehrenstein, G.W. (2001) *Polymeric Materials: Structure, Properties, Applications*. Munich, Germany: Hanser Publishers.

EOTA (2012) *Technical Report TR41. Non-reinforcing hexagonal geogrid for the stabilization of unbound granular layers by way of interlock with the aggregate, prepared by KIWA for the European Organisation for Technical Approvals (EOTA).*

Giroud, J.P., Ah-Line, C. and Bonaparte, R. (1984). *Design of unpaved roads and trafficked areas with geogrids. Proceedings of Conference on Polymer Grid Reinforcement. Thomas Telford. London. UK. pp 116–127.*

Giroud, J.P., & Han, J., 2004, Design Method for Geogrid-Reinforced Unpaved Roads. I. Development of Design Method, Journal of Geotechnical and Geoenvironmental Engineering, Vol. 130, No. 8, August 2004, pp. 775-786

Giroud, J.P., and Han, J., (2016). Mechanisms governing the performance of unpaved roads incorporating geosynthetics. Part 1. Geosynthetics. Feb/March 2016, Vol 34, No 1, pp. 23-33.

Giroud, J.P. (2009) *An assessment of the use of geogrids in unpaved roads and unpaved areas, Proceedings of the Jubilee Symposium Polymer Geogrid Reinforcement, Institution of Civil Engineers, London, UK, 2009, pp. 23-36*

Haliburton, T.A., Folwer, J. and Langan, J.P. (1980) *Design and construction of a fabric reinforced test section at Pinto Pass, Mobile, Alabama.* Washington, DC, USA: Trans. Res. Record no. 79.

Jenner, C.G., Watts, G.R.A., Blackman, D.I., (2002) *Trafficking of reinforced, unpaved subbases over a controlled subgrade. Seventh International Conference on Geosynthetics, vol. 3. Nice, pp. 931–934*

Jewell, R. A., Milligan, G. W. E., Sarsby, R. W. and Dubois, D. (1984) *Interaction between soil and geogrids. Proceedings of Symposium on Polymer Grid Reinforcement in Civil Engineering, London, UK pp 19-29.*

Kabir, M.H. (1984) *In-isolation and In-soil Behaviour of Geotextiles, Ph.D. Thesis, University of Strathclyde, Glasgow, UK.*

Kanyoza, A. (2003) Comparison of the efficiency of mesh elements and short fibres in micro reinforcement of granular soils. MPhil thesis, University of Strathclyde, Glasgow, UK.

Khan, A.J. (1999*) A reassessment of the design of the geosynthetic reinforced soil structures. Ph.D. Thesis, University of Strathclyde, Glasgow, UK.*

Koerner, R.M. (2009). *An Overview of Geogrids, Proceedings of the Jubilee Symposium Polymer Geogrid Reinforcement, Institution of Civil Engineers, London, UK, 2009, pp. 3-12*

Koerner, R.M. (2016). *Geotextiles: From Design to Applications. Woodhead Publishing Co., Cambridge, UK.*

Konietzky, H., te Kamp, L., Groeger, T. and Jenner, C., 2004. *Use of DEM to model the interlocking effect of geogrids under static and cyclic loading. Numerical Modelling in Micromechanics via Particle Methods. Shimizu, Y., Hart, R. & Cundall, P. (Eds.), A.A. Balkema, Rotterdam. pp 3–11.*

Kupec, J. (2004) *The Application of the ISE Approach to the Design of Geosynthetic Reinforced Soil Structures. Ph.D. Thesis, University of Strathclyde, Glasgow, UK.*

Lees, A. (2020). *The stabilising power of interlock*. [Online] Tensar International Limited. Viewed 8th June 2020. Available from http://info.tensar.co.uk/blog/the-stabilising-power-of-interlock

McGown, A., Andrawes, K.Z., Yeo, K.C and Dubois, D. (1984) *The load-strain-time behaviour of Tensar Geogrids. Proceedings of the Conference on Polymer Geogrid Reinforcement, London, UK, pp 11-17.*

McGown, A. and Ozelton, M.W. (1973), *Fabric mem- brane in flexible pavement construction over soils of low bearing strength. Civil engineering and public works review, UK, pp. 3-7.*

Mercer, F.B (1986) *Critical aspects of industrial and academic collaboration. The Royal Society Philips Lecture, London, UK.*

Milligan, G. W. E. (1981). *The use of mesh products to improve the performance of granular fill on soft ground. Report to Netlon Ltd. (OUEL) report No.1346/81. Oxford University Engineering Laboratory.*

Milligan, G. W. E. and Love, J. P. (1984). *Model testing of geogrids under an aggregate layer on soft ground. Proceedings of Conference on Polymer Geogrid Reinforcement. London, UK. pp 128-138.*

Müller-Rochholz, J.M., Jas, H. and Harting, U. (1994) *Effect of traffic loading on the long-term behaviour of geogrids. 5th International Conference on Geotextiles, Geomembranes and Related Products, Singapore, 5-9 September 1994, Vol 3, pp. 1177-1180.*

Murray, R.T. and McGown, A. (1982) *The selection of testing procedures for the specification of geotextiles. Second International Conference on Geotextiles, Las Vegas, USA, pp. 291-296.*

Nielsen, M. (No Date) *Statistical Process Control (SPC).* [online] Michael Nielson Consulting. Viewed 1st February 2020. Available from: https://www.statisticalprocesscontrol.info/glossary.html

Nimmersgern, M. (1994) *Large scale biaxial creep tests on a Polypropylene geogrid. Otto-Graf Journal, Germany, p. 137-147.*

Paul, J. (1994) *The Development, Testing and Reinforcement Applications of Geogrids. M.Phil Thesis, University of Strathclyde, Glasgow, UK.*

P.L.G. Research Limited. *Plastics Material Mesh Structure*. Inventor: Frank Brian Mercer. UK patent application GB2035191. 9th October 1980.

P.L.G. Research Limited. *Plastics Material Mesh Structure*. Inventor: Frank Brian Mercer. UK patent application GB2073090. 14th October 1981.

P.L.G. Research Limited. *Molecularly orientating plastics material*. Inventor: Frank Brian Mercer. UK patent application GB2073090. 26th April 1984.

Study.com. (2017) *Woven vs. Non-Woven Geotextile Fabric.* [online] Study.com. Viewed 30th January 2020. Available from: https://study.com/academy/lesson/woven-vs-non-woven-geotextile-fabric.html.

Soong.T.Y, Lord, A.E. and Koerner. R.M. (1994) *Stress relaxation behaviour of HDPE geomembranes. 5th International Conference on Geotextiles, Geomembranes and Related Products. Singapore. Vol 3. Pp 1121 - 1124.*

Tensar International Limited. (no date) *Tensar International Limited.* [online] Tensar International Limited. Viewed 2015. Available from: https://www.tensar.co.uk/Downloads

Tensar International Limited. (1998) *Physical Properties of Geogrids.* [online] Tensar International Limited. Viewed 31st January 2020. Available from: https://www.tensar.co.uk/Services/Knowledge-Centre/physical-properties-of-geogrids

Tensar International Limited. (2019) *Radial stiffness and its performance relationship, Internal Tensar International Report, unpublished. Tensar International Ltd, Blackburn, UK.*

Tensar International Limited. (2019) *Two independent research test results comparing geogrids by performance as reinforcement in the unbound pavement layers, Internal Tensar International Report, unpublished. Tensar International Ltd, Blackburn, UK.*

Tensar Technologies Limited. *Geogrid or Mesh Structure*. Anthony Thomas Walsh. GB2391832. 18th February 2004.

Tutumluer E., Al Qadi I. L. (2009) *Pavement Base Reinforcement with Geogrids – Modeling the Aggregate Interlock Mechanism, Geo-Strata, pp 28-30.*

Walsh, A.T. (2006) *Isogrid Project, Internal Tensar international Report, unpublished. Tensar International Ltd, Blackburn, UK.*

Watts, G.R.A., Blackman, D.I., & Jenner, C.G., 2004, *The performance of reinforced unpaved sub-bases subjected to trafficking, Proceedings of the Third European Geosynthetics Conference EUROGEO 3, Munich, Germany, pp. 261-266.*

Wilson-Fahmy, R. F. (1981) *The Prediction and Measurement of the Behavior of Soil-Geotextile Model Systems Acting in Plane Strain, Ph.D. Thesis, University of Strathclyde, Glasgow, UK.*

Withers, P. J. and Bhadeshia, H.K.D.H. (2001) *Material Science and Technology, Volume 17, pp 355-375.*

Wrigley, N.E., Austin, R.A., Harrison, P.E., (1999) *The long term strength of geogrid reinforcement. Proceedings of Geosynthetics '99, IFAI, Vol. 2, Boston, Massachusetts, USA, April 1999, pp. 711-721.*

Yeo, K.C. (1985) *The Behaviour of Polymeric Grids Used for Soil Reinforcement. Ph.D. Thesis. University of Strathclyde, Glasgow, UK.*

Young, R.J. and Lovell, P.A. (2011) *Introduction to polymers. 3rd edition. Florida, USA: CRC Press.*

Appendices

APPENDIX A1 – Uniaxial Q.C and Index Testing

Uniaxial Geogrids

Uniaxial index testing of uniaxial geogrids is carried out in accordance with the testing standard ISO 10319 (2015) but has two deviations away from the standard:

1) ISO 10319 Clause 5.2 - Strain may be measured without using an extensometer.

2) ISO 10319 Clause 6.3.3 -Specimens should be prepared 2 ribs wider and outer ribs severed

Fig A1.1 shows the sample geometry to be used. Sampling is based on International Standard ISO 9862 (2005).

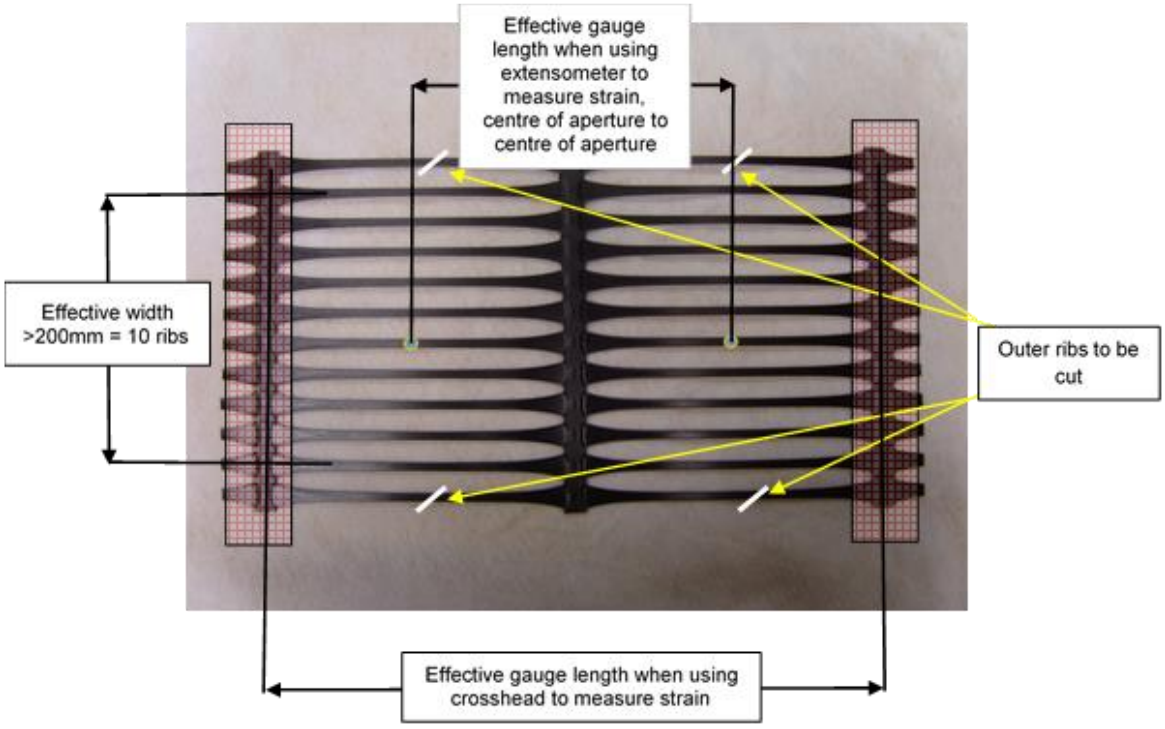


FIG. A1.1 – Sample geometry used for index testing uniaxial geogrids in accordance with ISO 10319.

The test specimen is placed into the tensile testing machine, as shown in Fig A1.2, taking into account the following key points that when clamping specimens in the jaws the:

- Samples are placed symmetrically in the jaws.
- Vertical ribs run as near as possible 90° to the jaws.
- Specimen is set parallel and well into the jaws.
- Outer ribs are severed before the test is started.
- Jaws are not out of square and interfering with the ribs.
- Transverse bar that is being gripped in the jaws is level with the hydraulic pistons/bolts that apply the pressure.



FIG. A1.2 – Uniaxial geogrid installed in the tensile testing machine.

The test is carried out at a strain rate of 20(±5)% of the gauge length with a pre-load no more than 1% of the maximum load. A minimum number of 5 specimens are tested.

The recorded results from the test are shown below in Table A1.1:

Required results	**Calculation used in result**
1) Maximum load (kN)	Taken directly from load cell, no calculation
2) Maximum strength (kN/m)	(Max load/no of ribs in specimen) x Ribs/m
3) Strain at maximum load (%)	Calculated in software using gauge length input
4) Strain at nominal strength	Calculated in software at a preset point load input
5) Secant stiffness at 2% Strain (kN/m)	(Strength @ 2% Strain x 100) / 2
6) Secant stiffness at 5% Strain (kN/m)	(Strength @ 5% Strain x 100) / 5
7) Secant stiffness at 10% Strain (kN/m)	(Strength @ 10% Strain x 100) / 10

Table A1.1. – Recorded results of a uniaxial geogrid index test.

Biaxial Geogrids

Uniaxial index testing of biaxial geogrids is carried out in accordance with the testing standard ISO 10319 (2015) but has two deviations away from the standard:

1) ISO 10319 Clause 5.2 - Strain may be measured without using an extensometer.

Fig A1.3 shows the sample geometry to be used for both machine direction (0°) and cross-machine direction (90°). Sampling is based on International Standard ISO 9862 (2005).

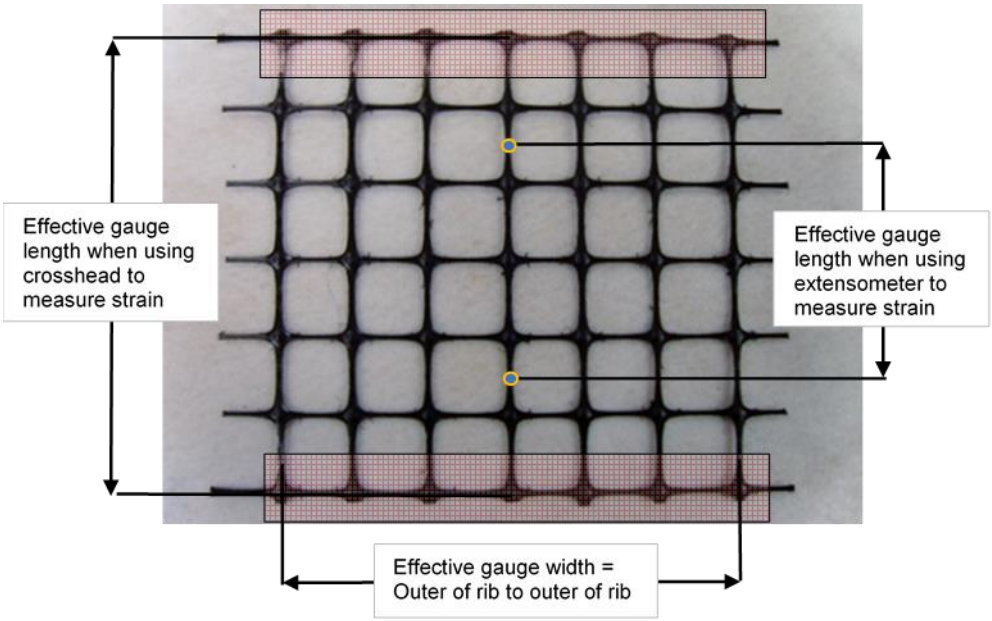


FIG. A1.3 – Sample geometry used for index testing biaxial geogrids in both the machine direction (0°) and cross-machine direction (90°) in accordance with ISO 10319.

The test specimen is placed into the tensile testing machine, as shown in Fig A1.4, taking into account the following key points that when clamping specimens in the jaws the:

- Samples are placed symmetrically in the jaws.
- Vertical ribs run as near as possible 90° to the jaws.
- Nodes are drawn up as close as possible to the jaw profile, before applying full pressure
- Relevant nodes are within clamps.
- Jaws are not out of square and interfering with the ribs.



FIG. A1.4 – Biaxial geogrid installed in the tensile testing machine.

The test is carried out at a strain rate of 20(±5)% of the gauge length with a pre-load no more than 1% of the maximum load. A minimum number of 5 specimens are tested in each direction (0° and 90°).

The recorded results from the test are shown below in Table A1.2:

Required results	**Calculation used in result**
1) Maximum load (kN)	Taken directly from load cell, no calculation
2) Maximum strength (kN/m)	Max load x (1000 / Width of sample)
3) Strain at maximum load (%)	Calculated in software using gauge length input
4) Strain at nominal strength (%)	Calculated in software at a preset point load input
5) Secant stiffness at 0.5% Strain (kN/m)	(Strength @ 0.5% Strain x 100) / 0.5
6) Secant stiffness at 2% Strain (kN/m)	(Strength @ 2% Strain x 100) / 2
7) Secant stiffness at 5% Strain (kN/m)	(Strength @ 5% Strain x 100) / 5
8) Secant stiffness at 10% Strain (kN/m)	(Strength @ 10% Strain x 100) / 10

Table. A1.2 – Recorded results of a biaxial geogrid index test.

Triaxial Geogrids

Uniaxial index testing of triaxial geogrids is carried out in accordance with the testing standard ISO 10319 (2015) and EOTA TR041 (2012) but has three deviations away from the ISO 10319 standard:

1) ISO 10319 Clause 5.2 - Strain may be measured without using an extensometer.

2) ISO10319 Clause 6.1 - Tested in four directions 0, 30, 60, 90°. The standard states only Machine Direction and Cross-Machine Direction

3) ISO10319 Clause 6.1 - 3 specimens tested in 30, 60° direction. The standard states only 5 in Machine Direction and Cross-Machine Direction.

Figs A1.5 and A1.6 show the sample geometry to be used for 0°/60° and 90°/30° directions respectively. Sampling is based on International Standard ISO 9862 (2005) and EOTA TR041 (2012).

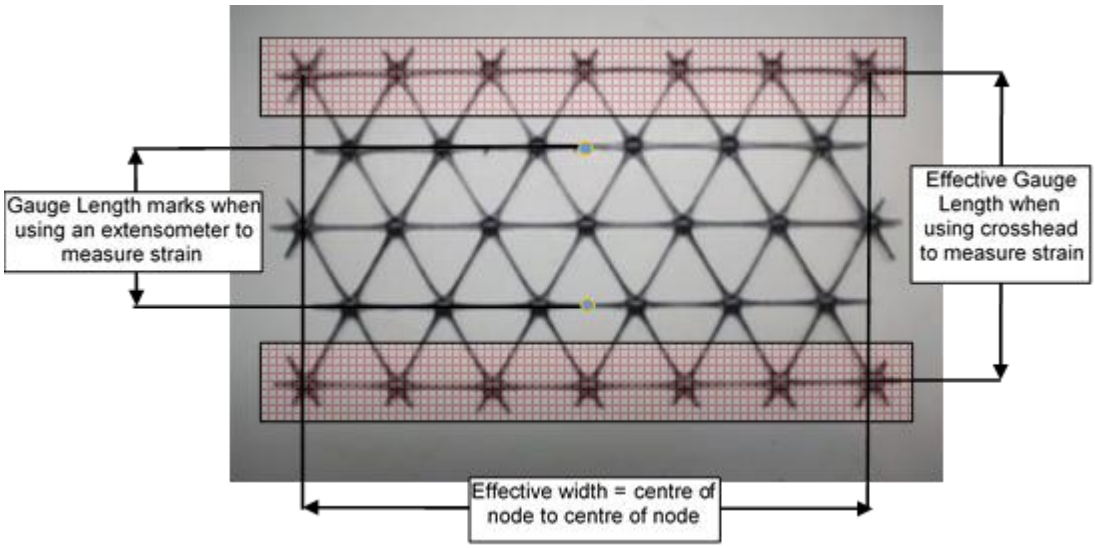


FIG. A1.5 – Sample geometry used for testing 0° and 60° directions

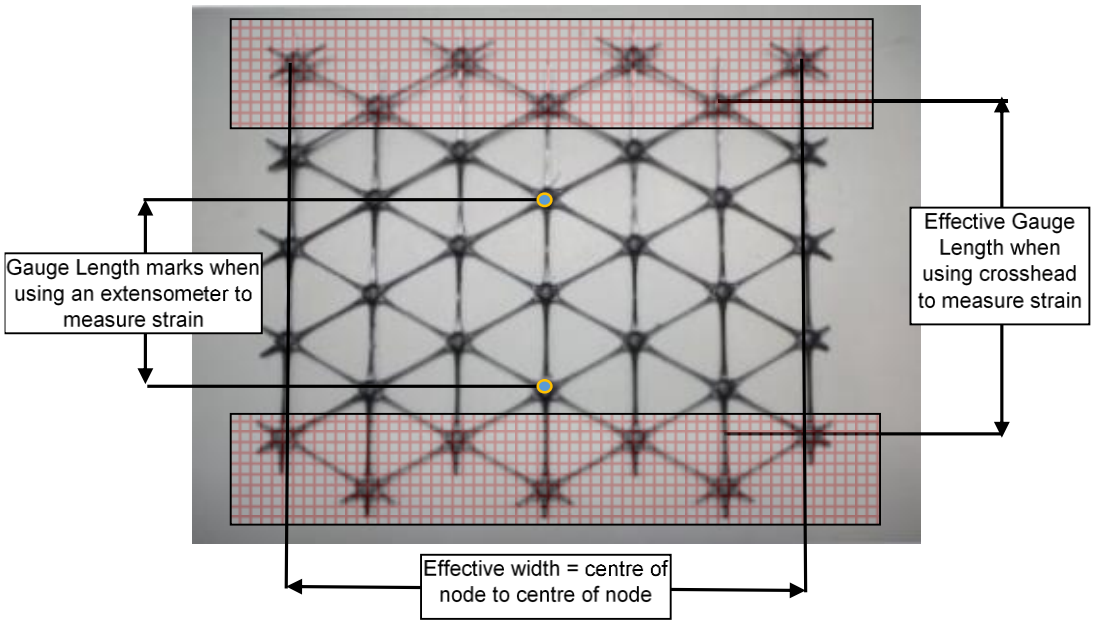


FIG. A1.6 – Sample geometry used for testing 90° and 30° directions

The test specimen is placed into the tensile testing machine, as shown in Fig A1.7, taking into account the following key points that when clamping specimens in the jaws the:

- Samples are placed symmetrically in the jaws.
- Vertical ribs of the 90° and 30° specimens run as near as possible 90° to the jaws.
- 0° and 60° specimens are set parallel and well into the jaws but without clamping the adjacent nodes
- Relevant nodes are clamped.
- Jaws are not out of square and interfering with the ribs.



FIG. A1.7. – Triaxial geogrid installed in the tensile testing machine.

The test is carried out at a strain rate of 20(±5)% of the gauge length with a pre-load no more than 1% of the maximum load. A minimum number of 5 specimens are tested in the 0° and 90° directions and a minimum number of 3 specimens are tested in the 30° and 60° directions.

The recorded results from the test are shown below in Table A1.3:

Required results	Calculation used in result
1) Maximum load (kN)	Taken directly from load cell, no calculation
2) Maximum strength (kN/m)	Max load x (1000 / Width of sample)
3) Strain at maximum load (%)	Calculated in software using gauge length input
4) Secant stiffness at 0.5% Strain (kN/m)	(Strength @ 0.5% Strain x 100) / 0.5
5) Secant stiffness at 2% Strain (kN/m)	(Strength @ 2% Strain x 100) / 2
6) Secant stiffness at 5% Strain (kN/m)	(Strength @ 5% Strain x 100) / 5
7) Secant stiffness at 10% Strain (kN/m)	(Strength @ 10% Strain x 100) / 10

Table. A1.3. - Recorded results of a triaxial geogrid index test.

APPENDIX A2 - Uniaxial Creep Testing

Below outlines the method for setting up and carrying out uniaxial creep tests.

Samples are cut from a roll of TriAx® TX160 in the directions specified in Fig A2.1 to the same dimensions as those used in Uniaxial Q.C and Index testing outlined in Appendix A1.

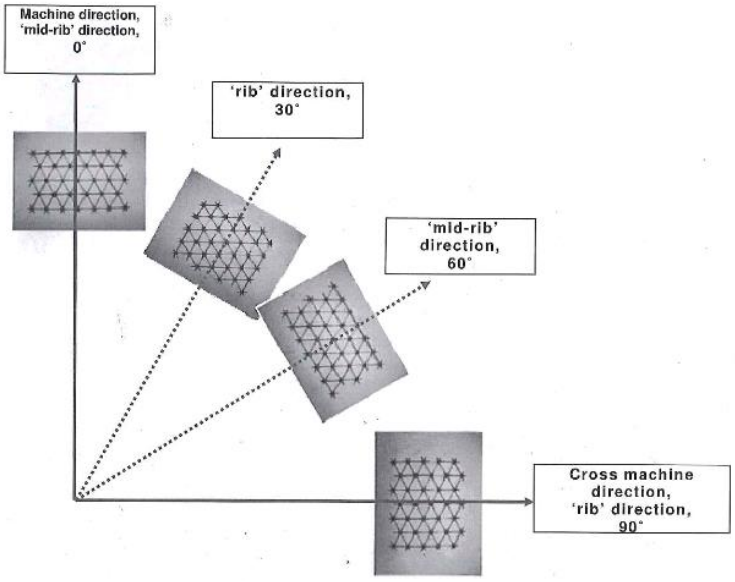


FIG A2.1 – Sample selection/testing directions, EOTA (2012).

The bottom compression jaw is set up perpendicular in a vice shown in Fig A2.2.

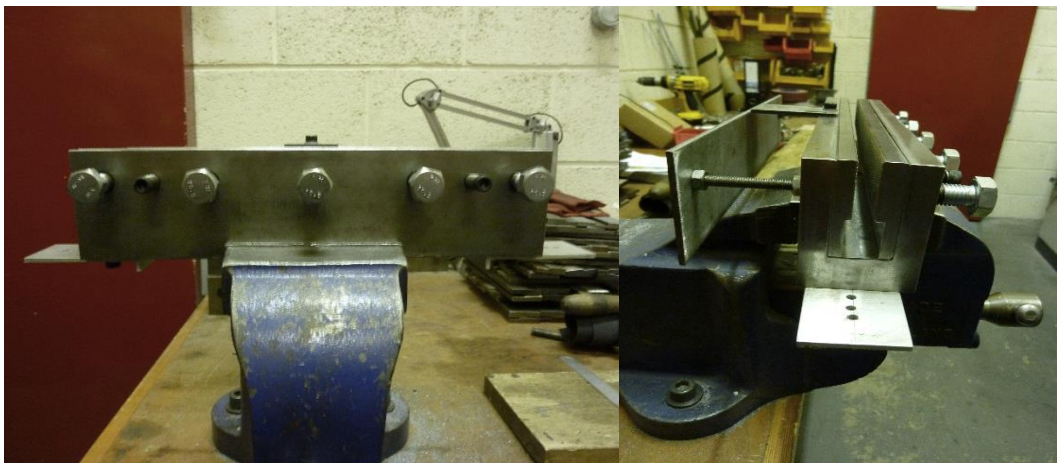


FIG A2.2 – Bottom compression jaw.

The grid is positioned in the jaw so that the grid is central and that the ribs are perpendicular to the jaw, shown in Fig A2.3. the grid is then gripped on the same nodes used for tensile testing shown in the EOTA TR041 and Appendix A1.

NOTE* A ruler is used to measure the distance from the outer ribs to the edge of the jaw to ensure that the grid is central.

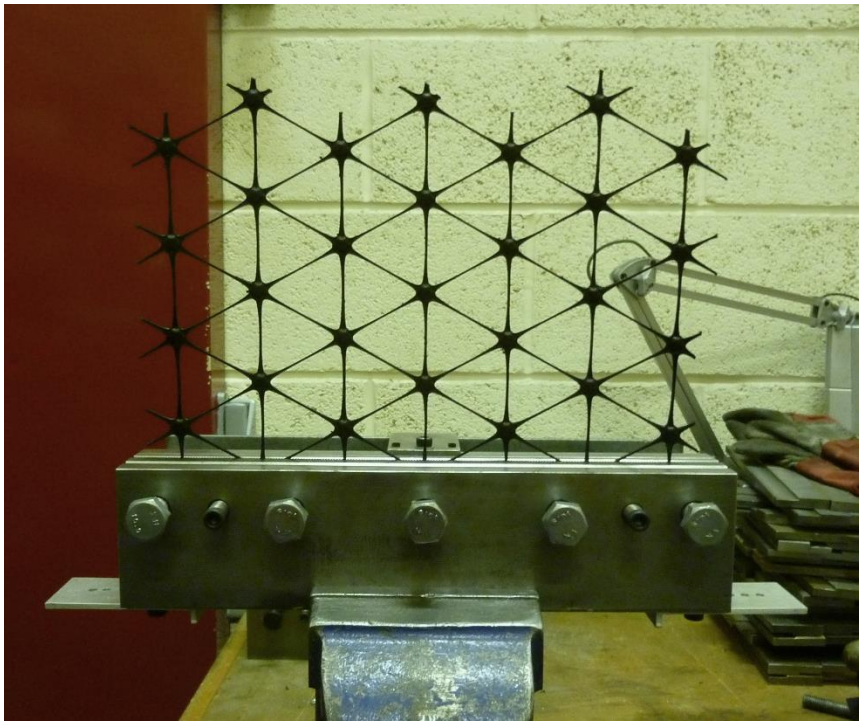


FIG A2.3 – 30° and 90° test specimen position in the bottom jaw.

Once central and positioned on the correct nodes the grid is secured by tightening the bolts to clamp the grid in position.

The load to be applied is added to a cradle. The load consits of the jaw, cradle, hanger and additional weights (lead & steel) until the desired load is reached. In this case 40kg. This is shown in Fig A2.4.

Note* The load is weighed using a calibrated 25kN load cell.

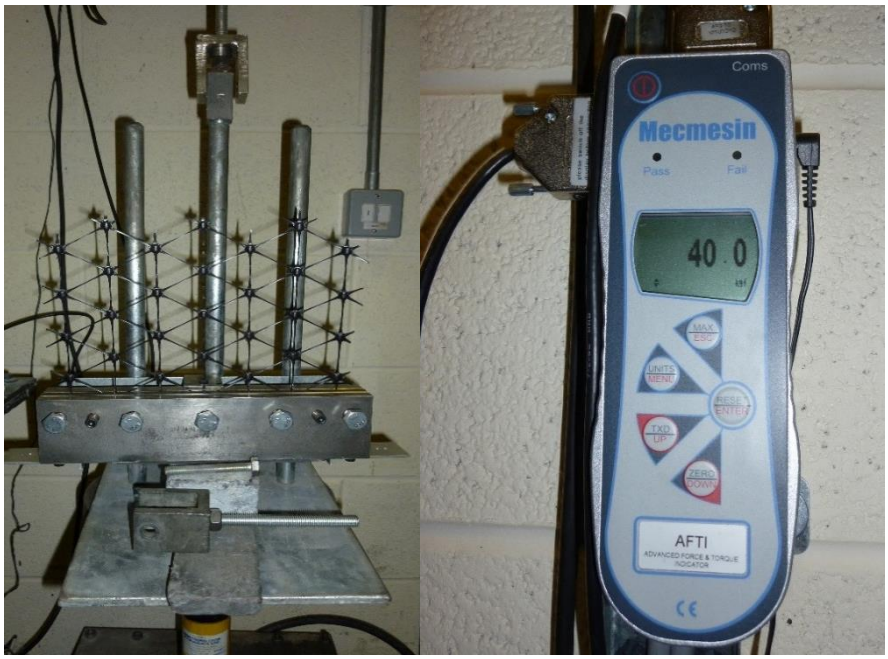


FIG A2.4 – Load consisting of a cradle, hanger and jaw with additional weights totalling 40kg.

The hanger and the jaw are then secured to the cradle and placed into position under the top jaw. This is shown in Fig A2.5.

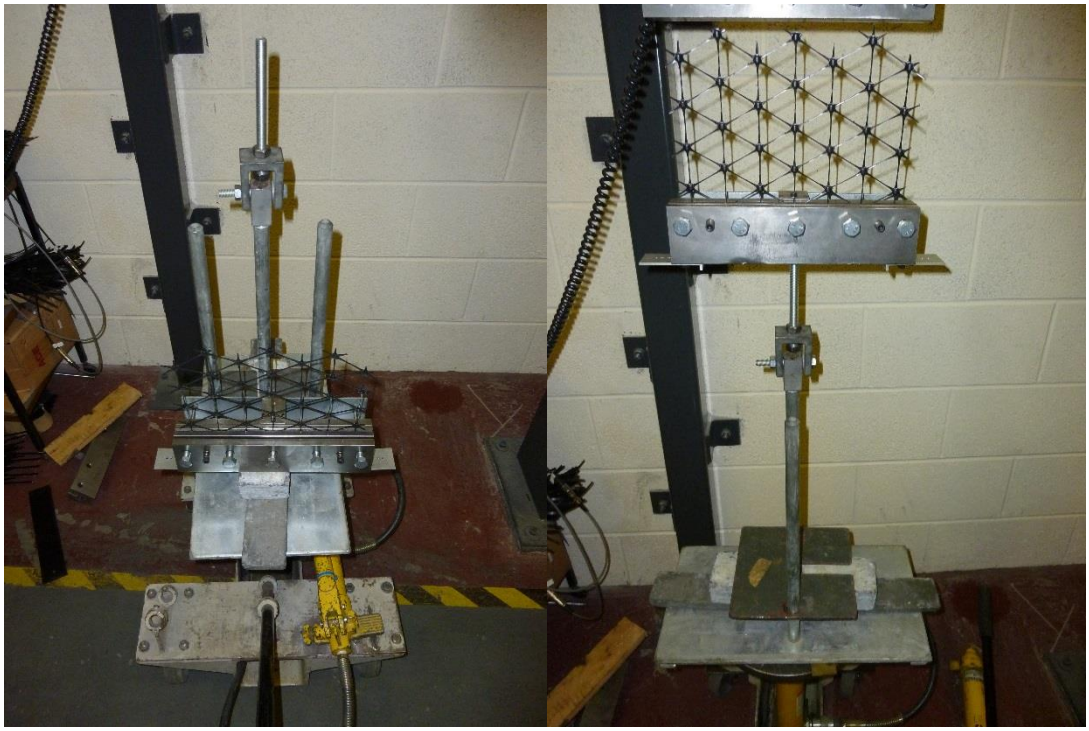


FIG A2.5 – Hanger and bottom jaw secured on the cradle.

The grid is then placed into position in the top jaw by jacking up the cradle until the nodes are in the correct position as seen in Fig A2.6.

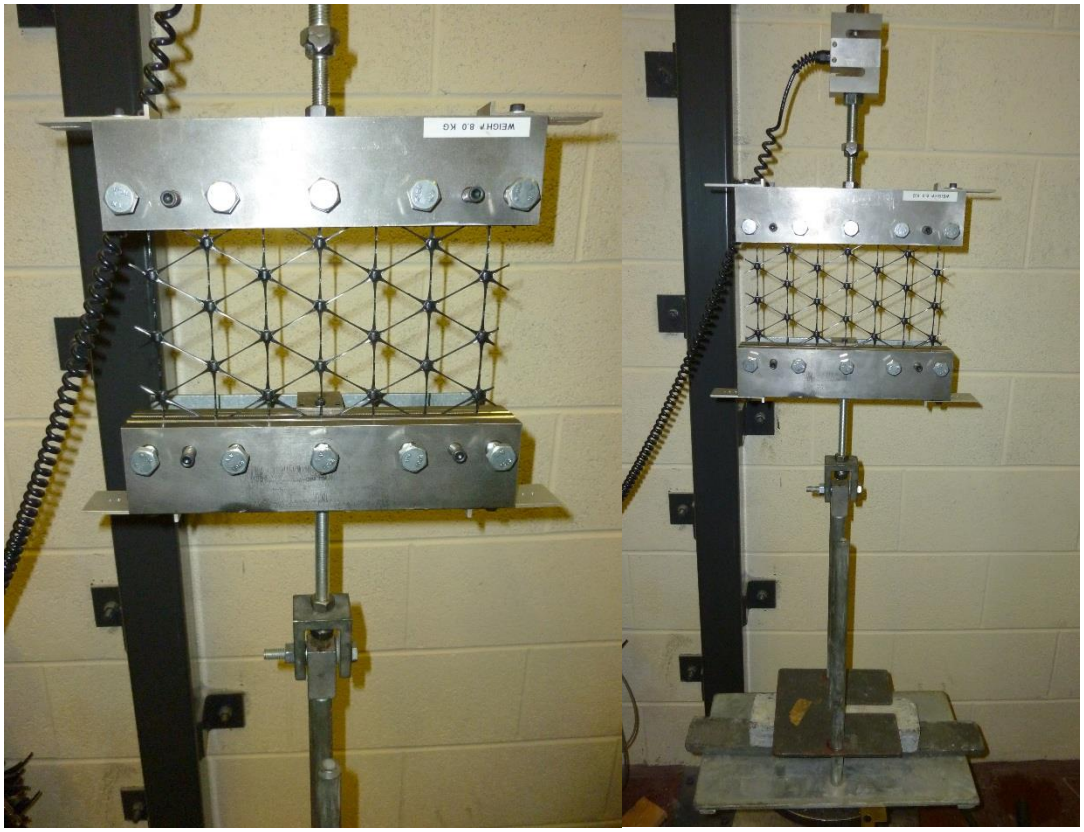


FIG A2.6 – Bottom jaw set up and geogrid positioned in the top jaw ready for clamping.

Before the grid is clamped into position, the LVDT's are added to the top jaw, but not secured, and the force gauge is turned on. This ensures the load cell above the jaw is tared off so that the load to be measured doesn't include the weight of the LVDT's and the top jaw. This is shown in Fig A2.7.

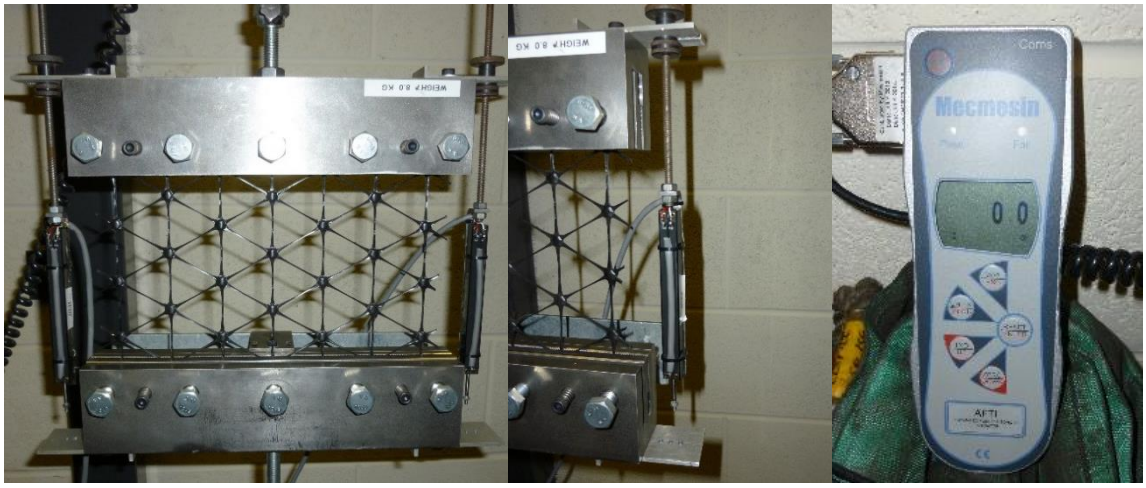


FIG A2.7 – LVDT's added to the top jaw but not secured and the force gauge turned on.

The grid is then clamped into position and the LVDT's are aligned so that they are perpendicular to the geogrid. The LVDT's are then secured to the tables on the bottom jaw and the plunger reset to allow sufficient travel and recording of strain. This is shown in Fig A2.8.

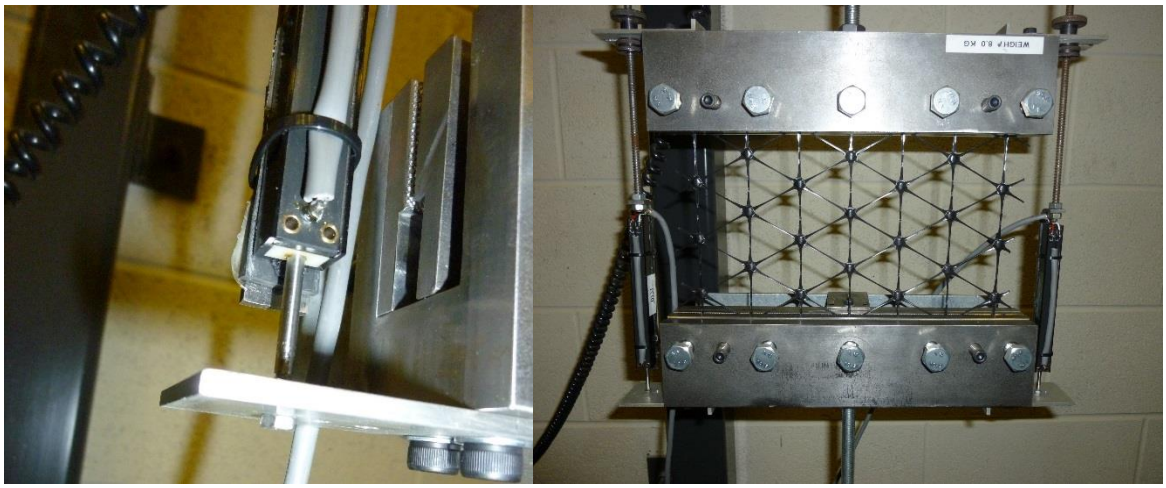


FIG A2.8 – Final clamped test specimen with LVDT's secured in place.

With the geogrid clamped and the LVDT's added the load will be in slight compression according to the force gauge. The jack on the trolley is released slowly until the load on the gauge reads 0.0kg. An example of this is shown in Fig A2.9.



FIG A2.9 – Force gauge showing slight compression on clamped geogrid. Load is slow released until forge gauge reads 0.0kg.

When the gauge is reading 0.0kg the gauge length can be measured. The gauge length is measured using a tape measure from the table on the top jaw to the table on the bottom jaw. The example in Fig A2.10 shows a gauge length of 289mm.

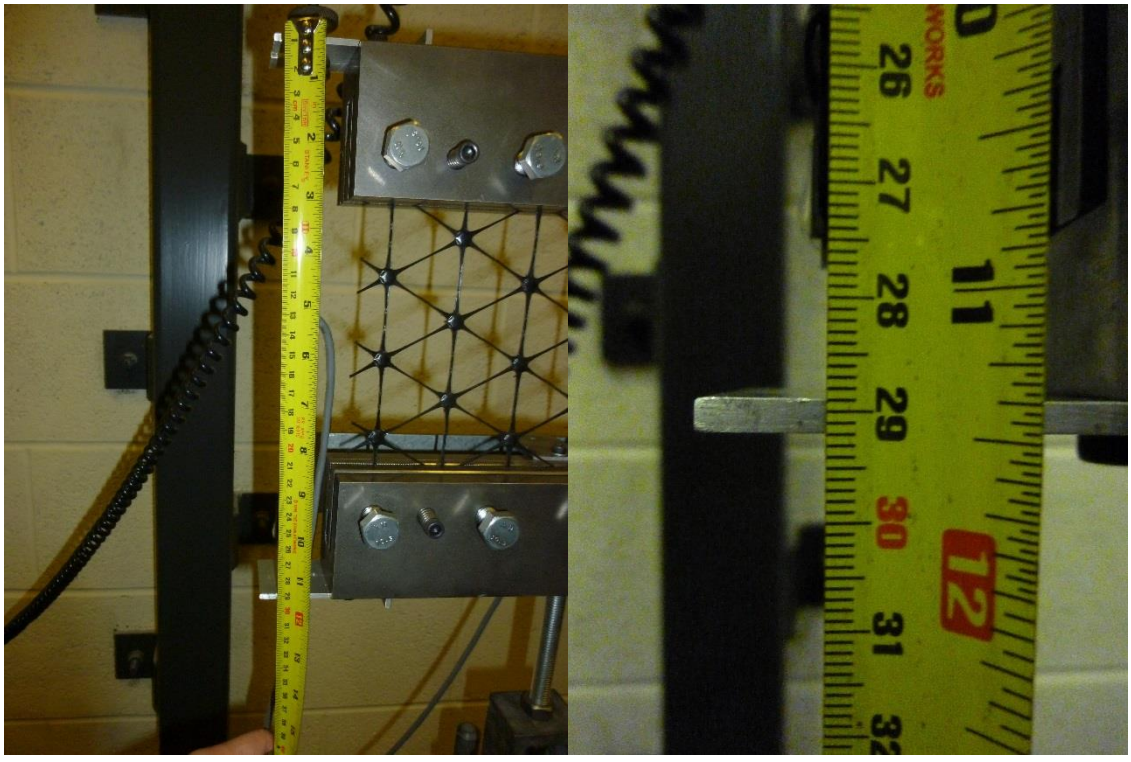


FIG A2.10 – Gauge length reading of test specimen prior to testing.

This is measured on both sides and the average is taken as the gauge length.

This gauge length is then added to the data logging software so that the strain can be calculated. The starting logging frequency is set at the minimum which is every 2 seconds. The sensors (LVDT's) are tared off to read 0.00mm. This is all shown in Fig A2.11.

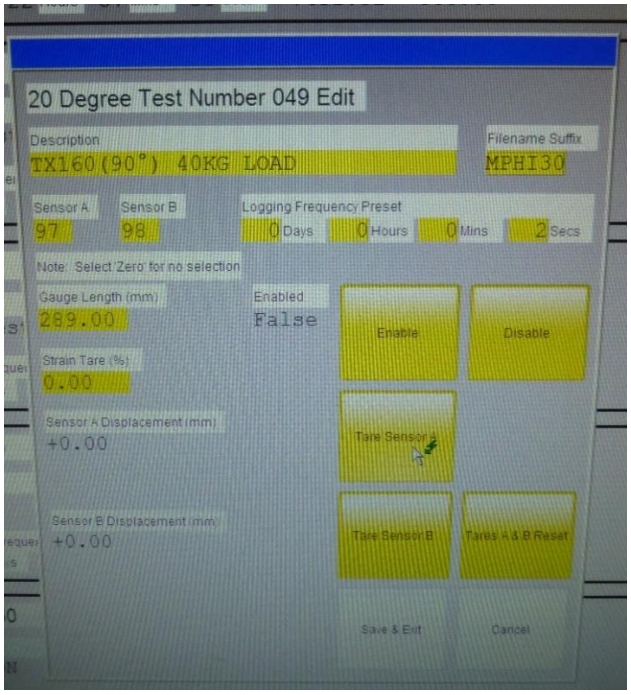


FIG A2.11 – Data logging software set-up page with gauge length added, logging frequency set and sensors (LVDT's) tared off.

The test is then enabled, and the test begins logging data. The load is then released smoothly and will come off the trolley within the first 2 to 3 seconds. The load on the force gauge (attached to the test) should read the same as when the load was weighed out, shown in Fig A2.12



FIG A2.12 – Test under load with force gauge reading.

Over time the test will record strain and the logging frequencies can be changed accordingly. The frequencies used are:

- 2 seconds for the initial 6 minutes.
- 30 seconds after 6 minutes.
- 1 minute after 12 minutes.
- 6 minutes after 1 hour
- 12 minutes after 2 hours until completion.

The tests run for a minimum of 24 hours and then terminated. Before termination the logging frequency is changed to every 2 seconds and the trolley is slowly jacked up until the load is taken off the specimen. The test is then disabled, and the data is analysed/plotted accordingly.

APPENDIX A3 – Quadrant Radial Creep Testing

There are currently no testing standards available, and no such testing has been carried out for radial creep testing of triaxial geogrids.

Below outlines the method used for setting up and carrying out radial creep tests.

Figs A3.1 and A3.2 show the sample size and geometry for the 0°/60° direction and the 30°/90° direction quadrant radial test specimens respectively.

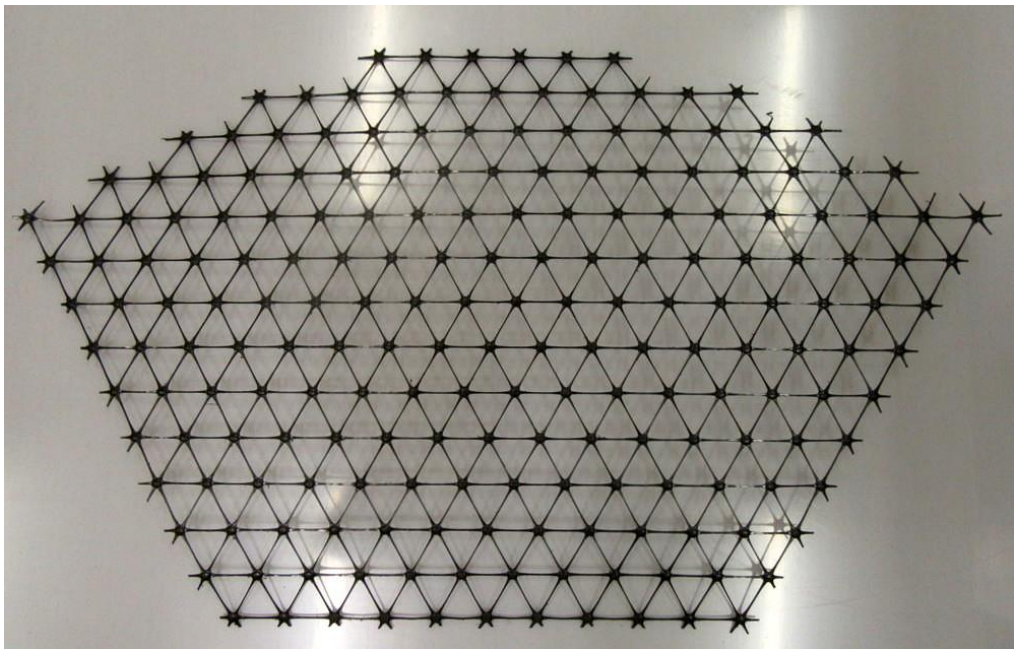


FIG A3.1 – Sample geometry used for 0° and 60° direction test specimens.

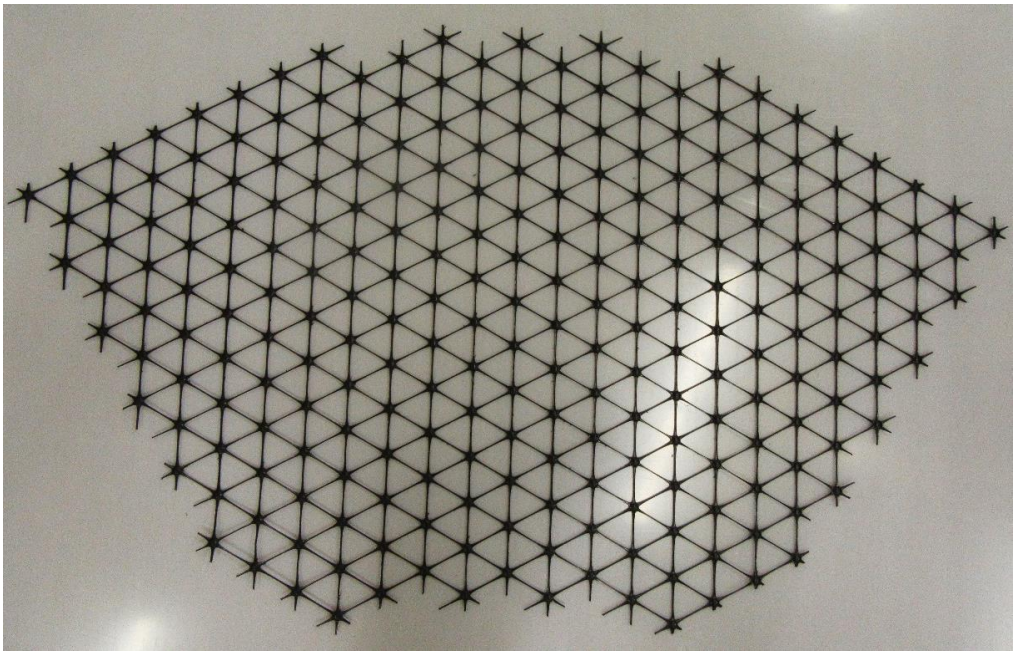


FIG A3.2 – Sample geometry used for 30° and 90° direction test specimens.

The samples are installed into the quadrant radial creep testing rig, which consists of one fixed inner clamp and 3 non-fixed outer clamps. The sample is installed in the fixed inner clamp with the centre line/ribs/nodes of the specimen being in-line with the centre bolt of the clamp. All the bolts are hand tightened with a spanner until the specimen is firmly clamped but not so that the nodes/ribs are damaged. The 25mm x 25mm square printed surface also aids in getting the sample/ribs/nodes straight. Fig A3.3 to A3.6 shows the specimens (for all directions) installed in the fixed inner clamp and outer clamps.

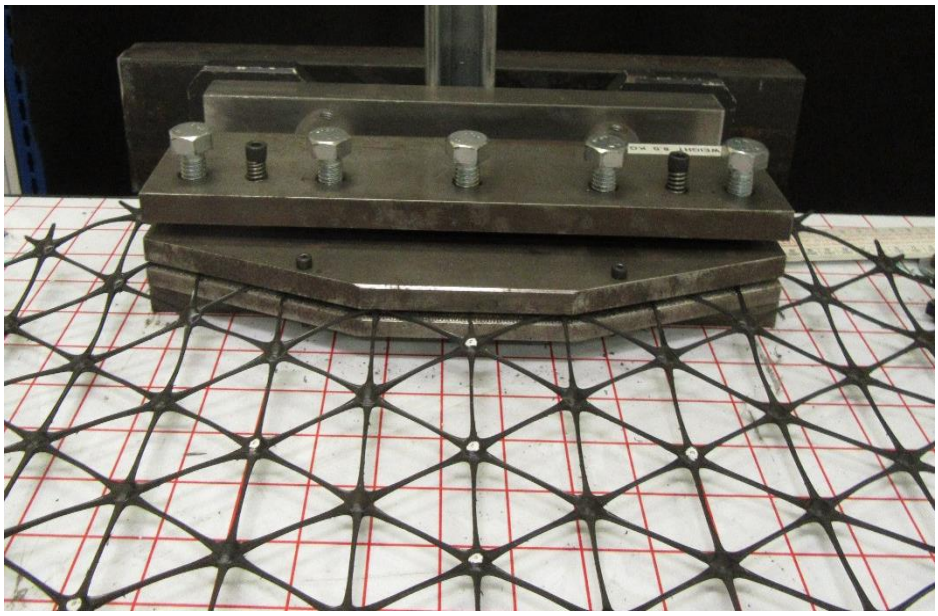


FIG A3.3 – 30°/90° specimen installed in the fixed inner clamp.

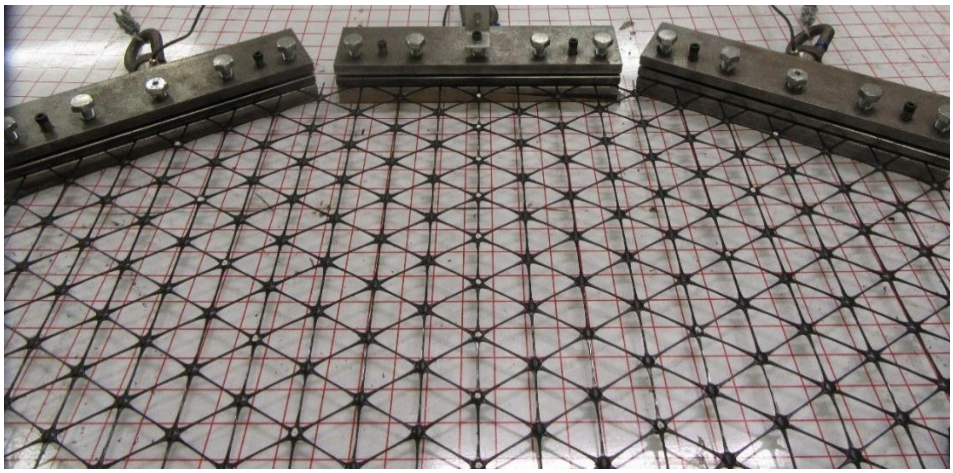


FIG A3.4 – 30°/90° specimen installed in the outer clamps.

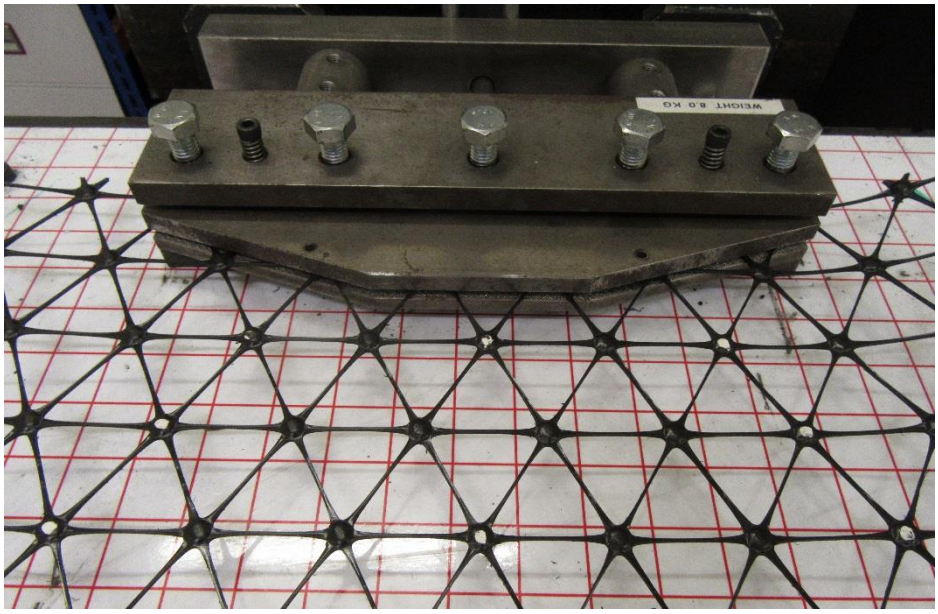


FIG A3.5 – 0°/60° specimen installed in the fixed inner clamp.

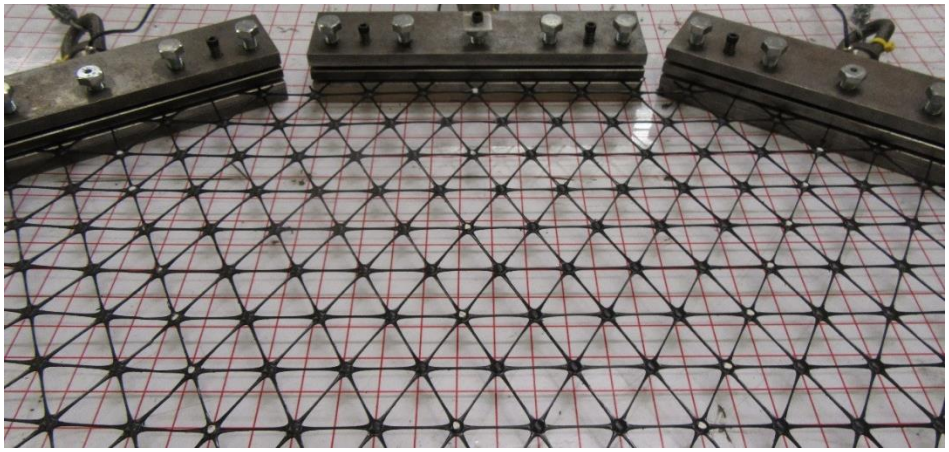


FIG A3.6 – 0°/60° specimen installed in the outer clamps.

Once the specimen is installed in the clamps the slack of the specimen is removed by sliding the outer clamps back away from the fixed clamp until the specimen is under tension. Once under tension the edge restraints are applied.

The edge restraints consist of a tab were one end has four bolts/pins that secure around the node of the geogrid and the other end attached to an eye and hook turnbuckle, this can be seen in A3.7

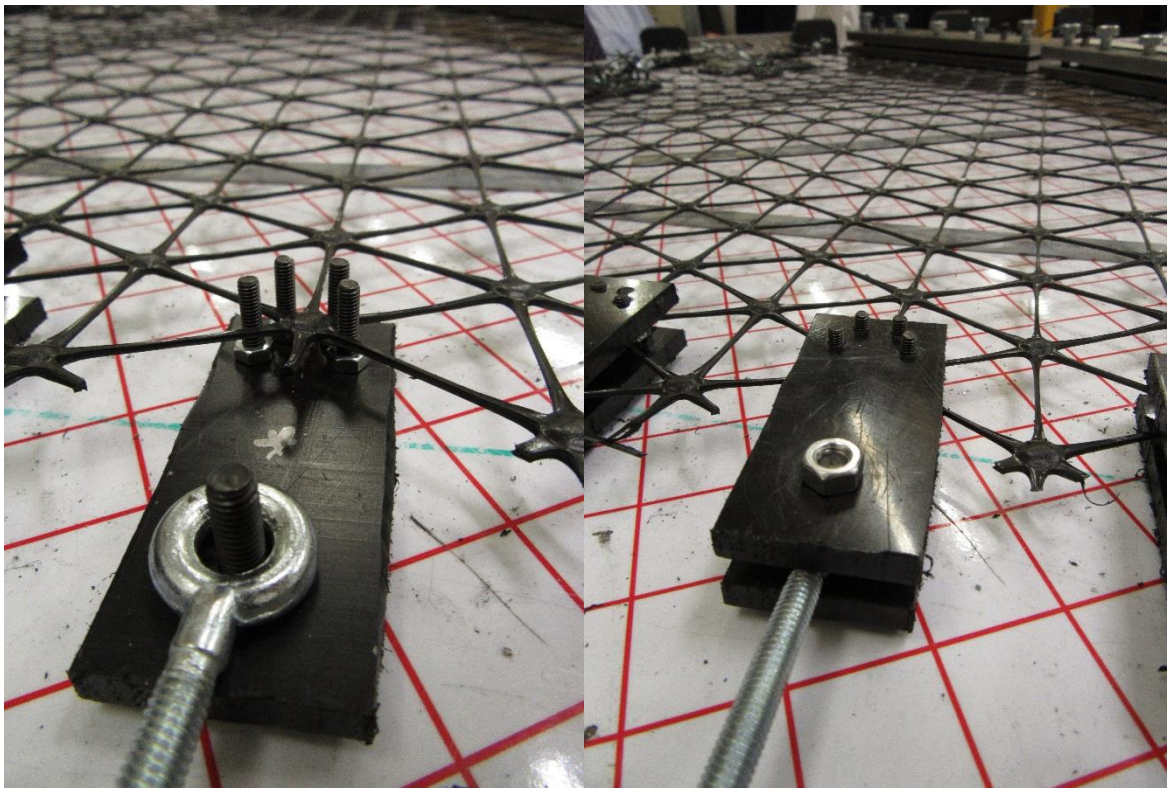


FIG A3.7 – Restraining tab consisting of four bolts/pins securing the node and attached to a turnbuckle.

Once all the tabs have been attached the turnbuckles are adjusted and hooked onto an edge restraining bar. This is carried out on both sides of the sample before any adjustments/tensioning is made. Fig A3.8 shows one side of a sample fitted with restraining tabs and the turnbuckles hooked onto an edge restraining bar.

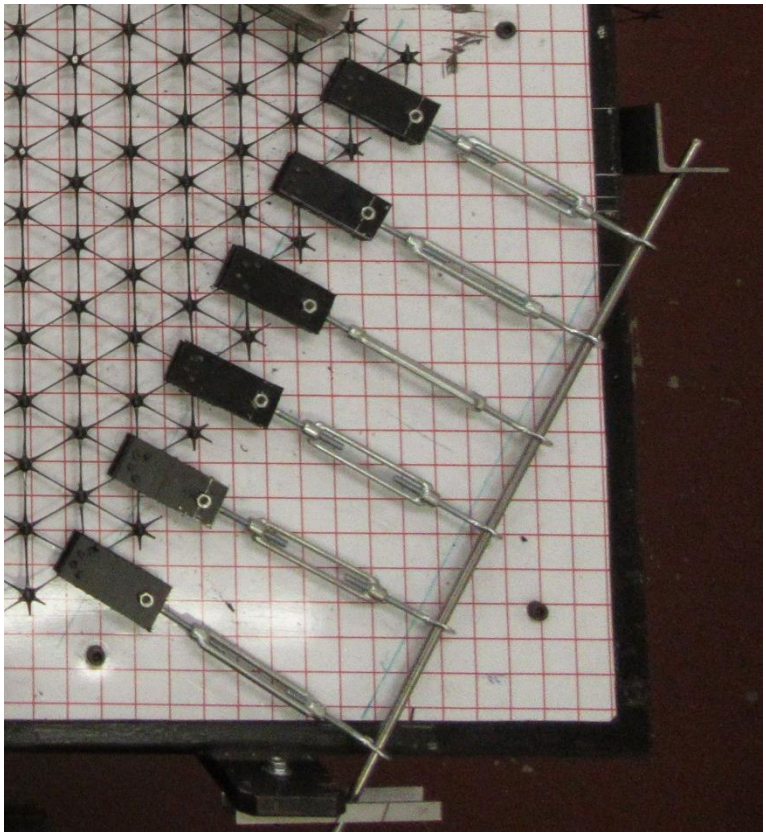


FIG A3.8 – Edge restraining set up consisting of tabs and turnbuckles attached to an edge restraining bar.

When all the tabs and turnbuckles have been attached the turnbuckles are adjusted so that tension is applied to the sample evenly. This is achieved by going around the specimen and carefully tightening all the turnbuckles by hand until even tension has been applied and no more tension can be placed on the turnbuckle without excessive force, they should be finger tight.

The central nodes of each outer clamp are marked white with a black dot placed in the centre of the node, this helps with any measurements that may be required if taking measurements from photographs, and a ruler is added down the centre line of the outer clamps underneath the specimen for scale purposes.

Fig A3.9 and Fig A3.10 show the finished set-up of a restrained specimen for 30°/90° directions and 0°/60° directions respectively.

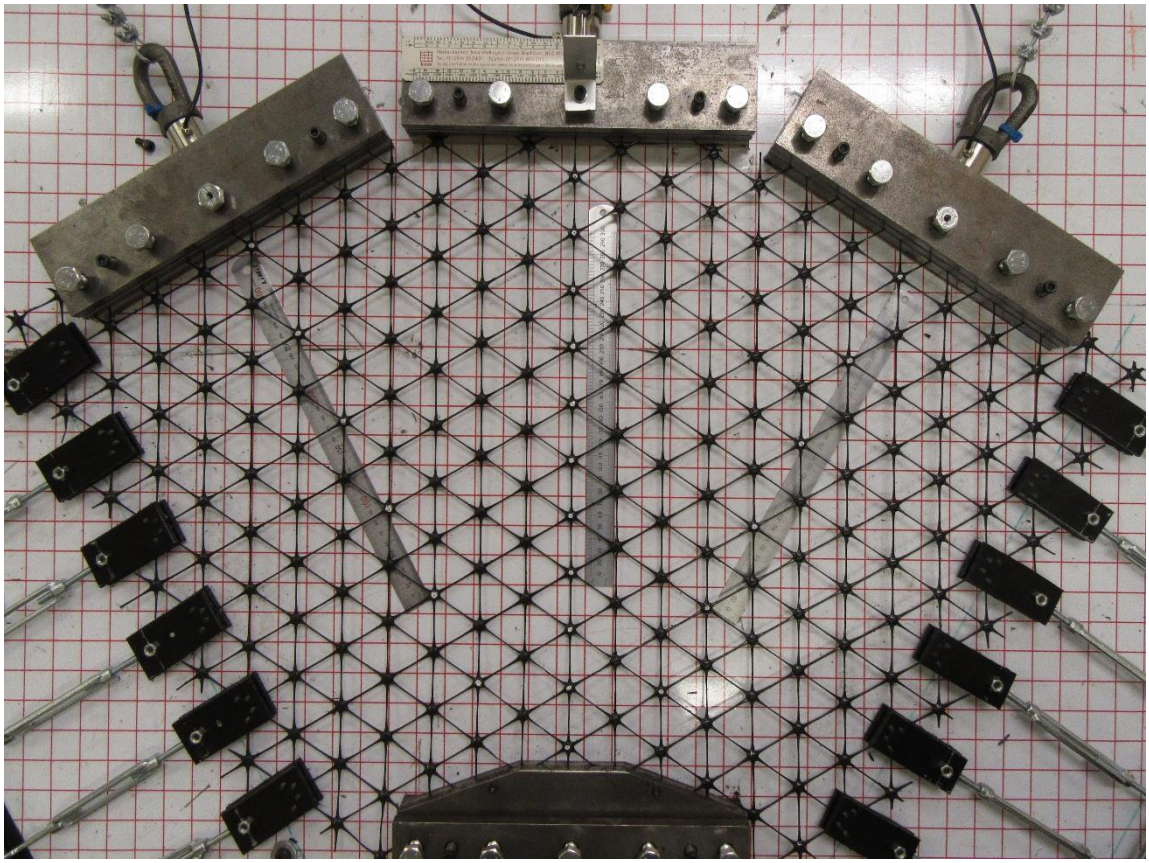


FIG A3.9 – Restrained sample set-up for 30°/90° direction.

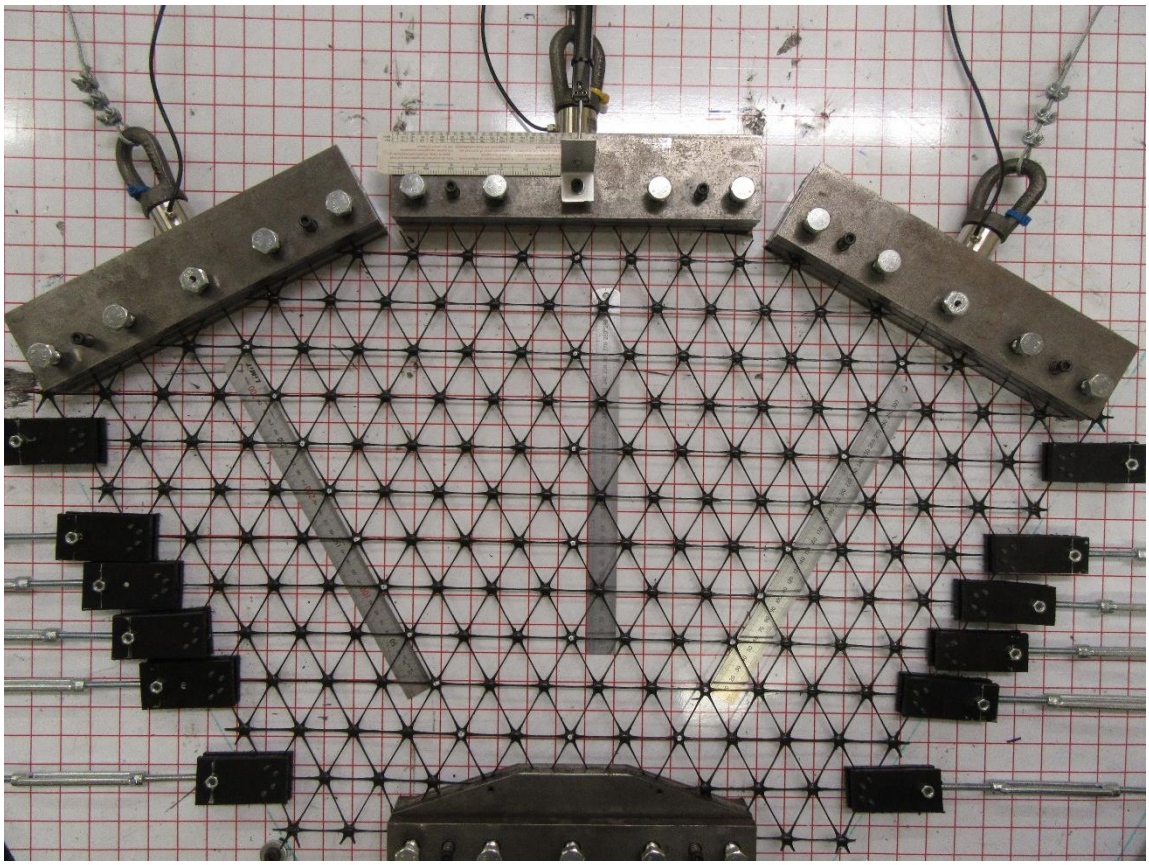


FIG A3.10 – Restrained sample set-up for 0°/60° direction

A LVDT is then attached to the central outer clamp as strain will only be measured from this position. This is shown in Fig A3.11.

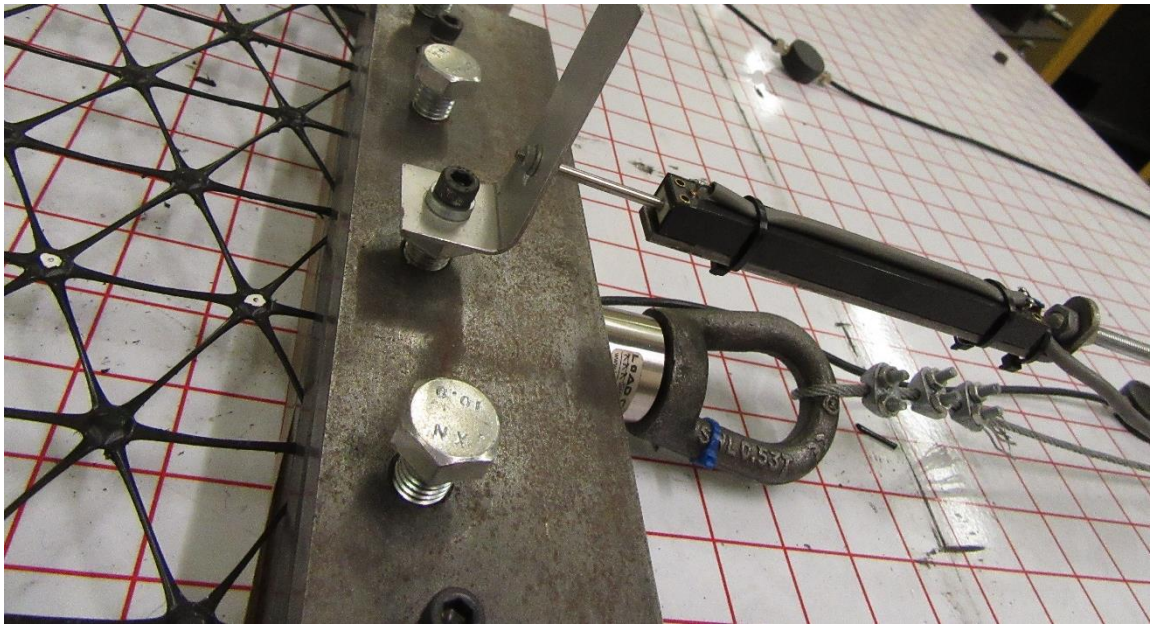


FIG A3.11 – LVDT attached to the central outer jaw.

A camera is also attached to a bracket above the test specimen to take photographs at intervals throughout the test. Fig A3.12.

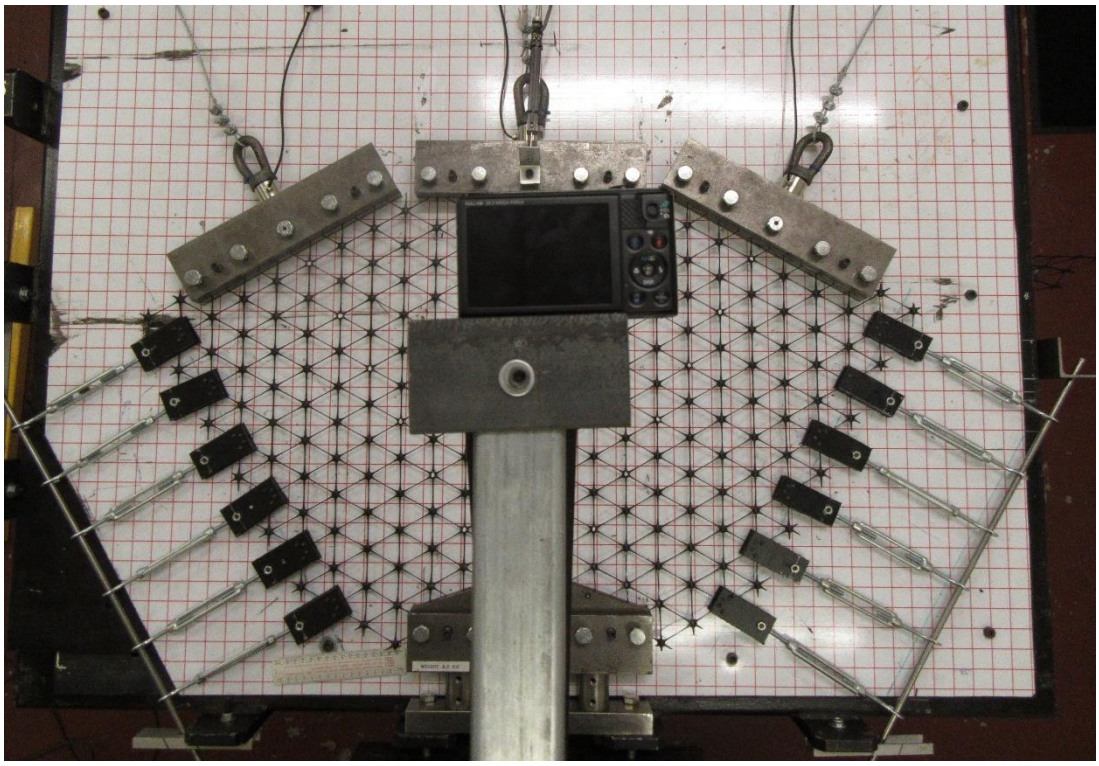


FIG A3.12 – Camera fixed on a bracket above the test specimen.

With the specimen installed and restrained the loads are set-up and positioned ready for the test to begin.

The three loads are built up on cradles and individually weighed using a calibrated load cell. Fig A3.13 and Fig A3.14 shows a cradle set-up and load cell reading.



FIG A3.13 – Cradle set-up.

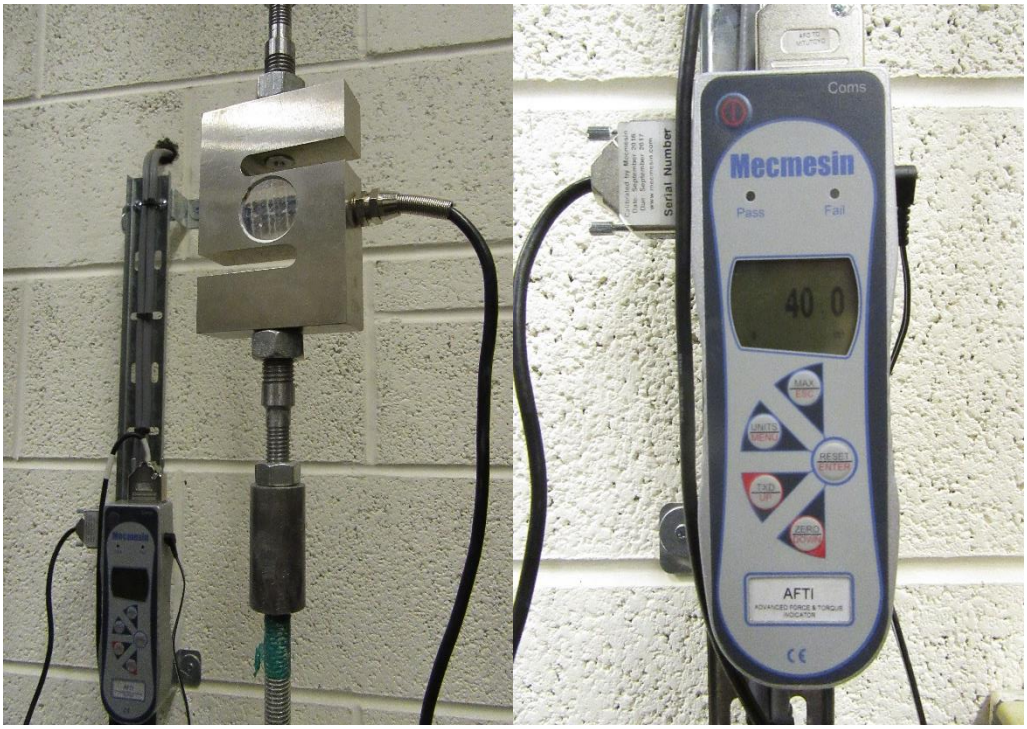


FIG A3.14 – Load cell and AFTI gauge reading 40.0kg.

The three loads are placed on a steel beam supported on a pallet truck. The loads are maneuvered into position so that they are directly under and in-line with the pulleys/turnbuckles. The cradles are then raised up on the pallet truck until the turnbuckles can be hooked onto the cradles via cables shown in Fig A3.15.

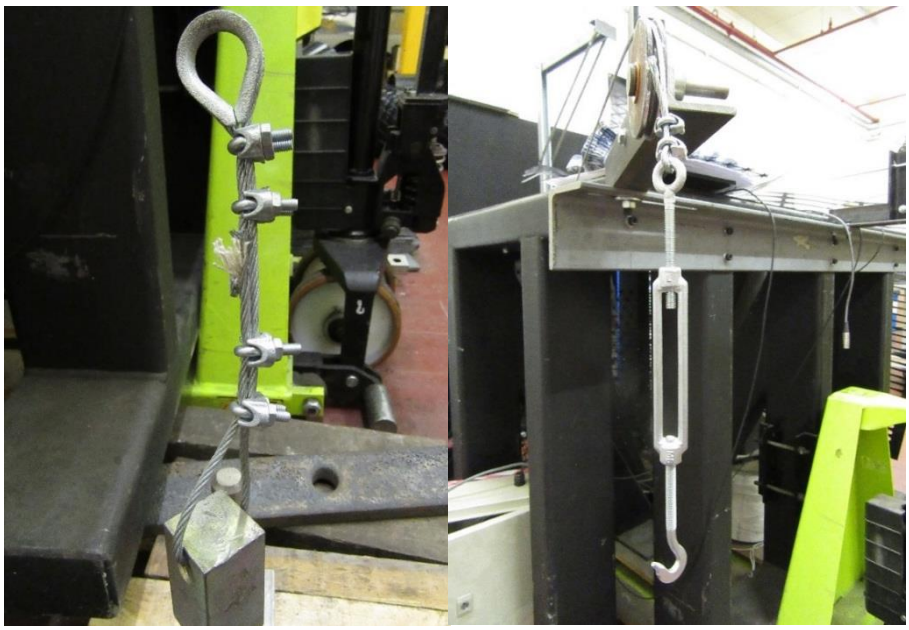


FIG A3.15 – Turnbuckles and cables used to support the load during testing.

Once the cradles are in-line with the pulleys and attached to the turnbuckles the turnbuckles are adjusted until the tension is removed from the cables attached to the outer jaws. The turnbuckles should be adjusted so that they are finger tight to a point where no more adjusting can be easily by hand made unless excessive force is applied. Fig A3.16 shows the cradles in-line and attached to the turnbuckles ready for the load to be applied.

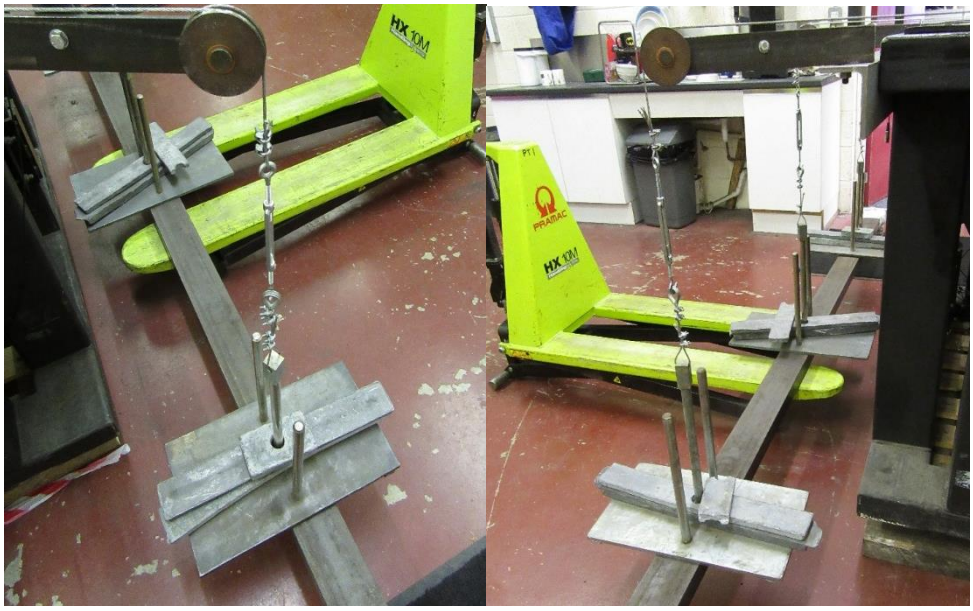


FIG A3.16 – Cradles attached to the turnbuckles, tensioned, and ready to start.

Once the cradles are under tension the edge restraints are double checked to ensure tension has not been removed from the test specimen and adjustments are made where necessary.

After all checks have been carried out and adjustments made, a starting photograph of the specimen is taken. The LVDT and logging system is then set-up and started to log data at a frequency of every 2 seconds.

With a stopwatch ready, the pallet truck is lowered slowly and controlled until the loads are released off the steel beam and the loads are fully applied to the test specimen. As soon as the loads are released the stopwatch is started.

Photographs are then taken at intervals of 30 seconds, 1 minute, 1 hour and before the test is terminated. The 30 seconds, 1 minute, and 1 hour photographs are taken with the stopwatch shown in the photograph as seen in Fig A3.17.

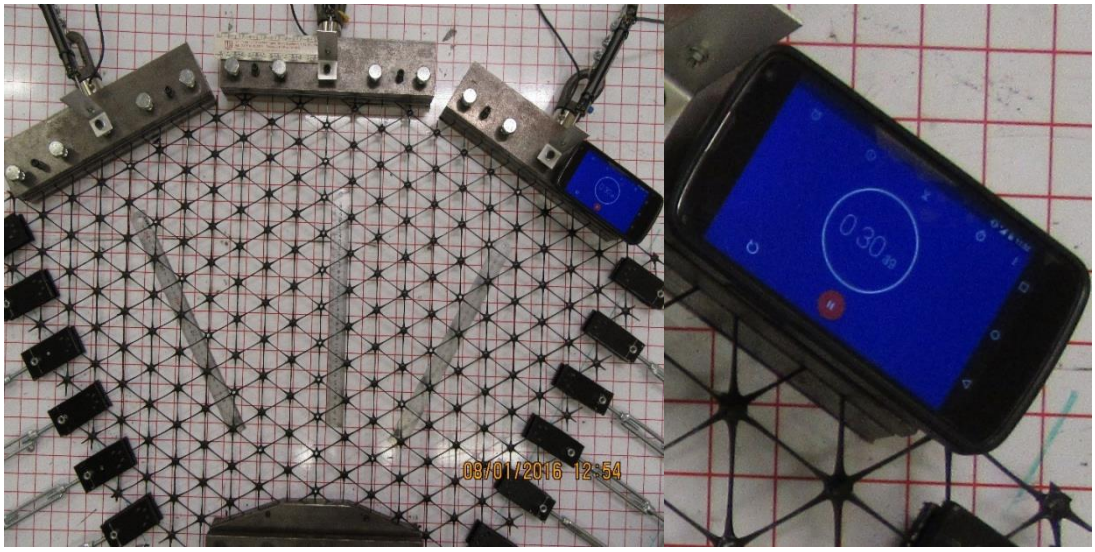


FIG A3.17 – Photograph of test specimen taken with stopwatch in view.

Once the required test duration is reached the pallet truck and steel beam is positioned back under the cradles and raised up until the loads are removed from the test.